BP23C7: high-yield synthesis and application in constructing [3]rotaxanes and responsive pseudo[2]rotaxanes

Manisha Prakashni[a] and Suvankar Dasgupta [a]*

Department of Chemistry, National Institute of Technology Patna, Patna – 800005, India

Electronic Supplementary Information

Table of Contents

1. Optimization table for BP23C7 synthesis

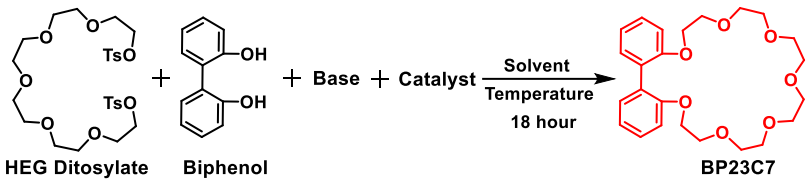

Entry	Solvent[b]	Base (equiv.)	Catalyst (equiv.)	Temperature	Yield (%)[c]
1	THF	NaH (3)	KPF_6 (0.25)	Room temp.	44
2	THF	NaH (6)	KPF_6 (0.25)	Room temp.	25
3	DMF	NaH (3)	KPF_6 (0.25)	Room temp.	23
4	DMF	NaH (6)	KPF_6 (0.25)	Room temp.	15
5	THF	NaH (3)	KPF_6 (0.25)	80°C	83
6	THF	NaH (3)	KI (0.25)	80°C	77
7	THF	K_2CO_3 (3)	-	80°C	66
8	THF	KO^{t}Bu (3)	-	80°C	71
9	THF	Cs_2CO_3 (3)	-	80°C	71
10	DMF	NaH (3)	KPF_6 (0.25)	80°C	51
11	DMF	Cs_2CO_3 (3)	-	80°C	64
12	ACN	Cs_2CO_3 (3)	-	80°C	86

[a]100 mg scale of HEG ditosylate has been used throughout. [b]THF = Tetrahydrofuran, DMF = N,N'-Dimethylformamide and ACN = Acetonitrile. [c]Isolated yield.

Table S1. Optimization reaction condition for **BP23C7** synthesis. Heating condition afforded better yields. Three equivalents of base worked better than six equivalents of base. Templates such as KPF_6 and KI are effective, and bases comprising of alkali metal ions performed additional role of templating. Cs_2CO_3 in acetonitrile medium at 80°C afforded the highest yield (86%, entry 12).

2. Nominal ESI-MS of a 1:1 mixture of DBA·PF_6 & BP23C7

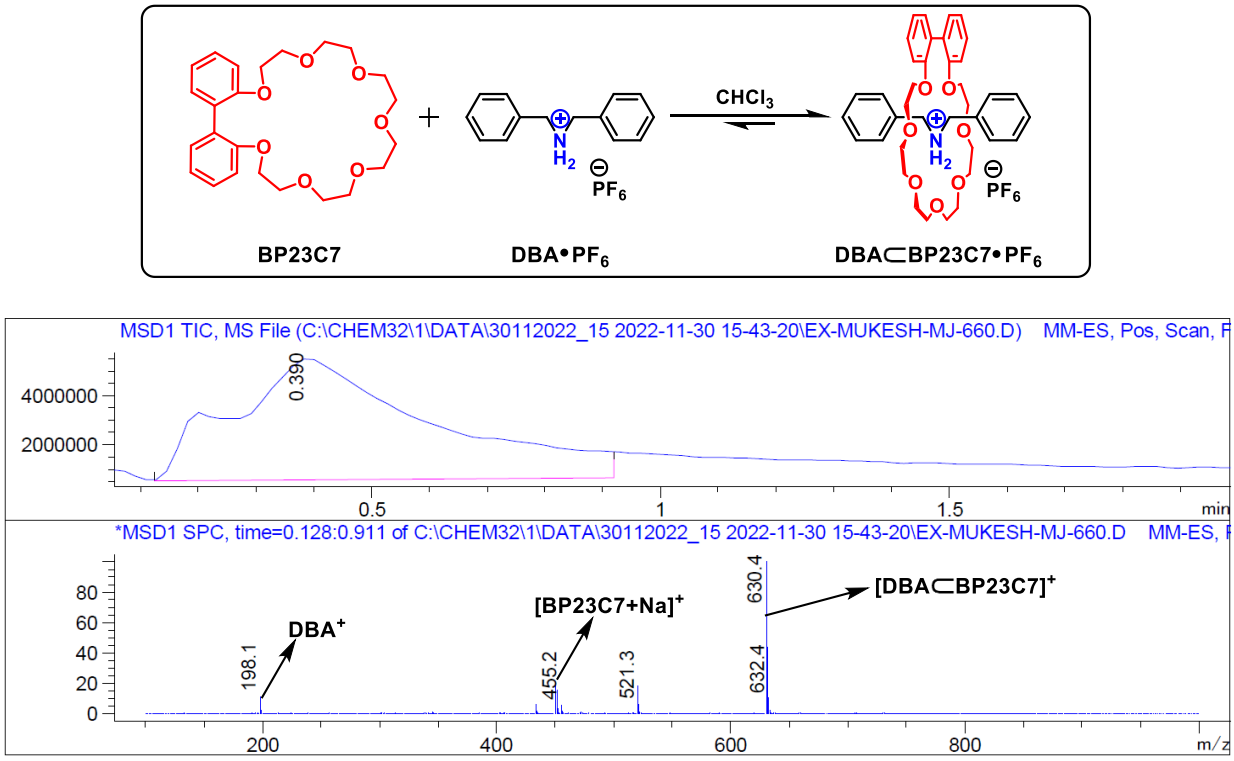

Figure S1. ESI mass spectrum of the equimolar mixture of **DBA·PF_6 & BP23C7** displayed base peak at *m/z* = 630.4 $[M\text{-}PF_6]^+$, where "M" corresponds to the pseudo[2]rotaxane species **DBA⊂BP23C7·PF_6**.

3. ^{1}H NMR spectrum of a 1:1 mixture of DBA·PF$_6$ & BP23C7

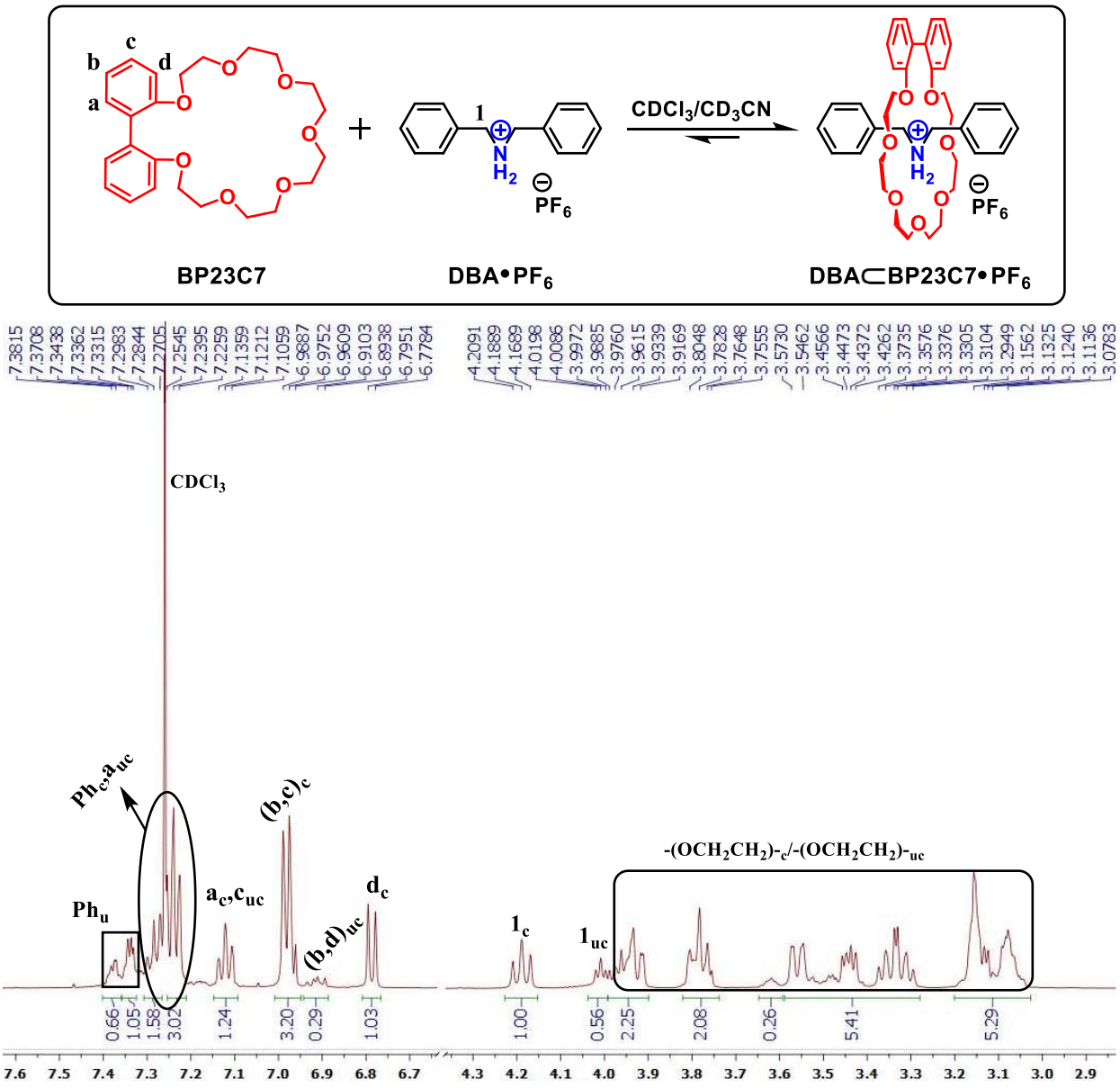

Figure S2. ^{1}H NMR spectrum (500 MHz, $CDCl_3/CD_3CN$ = 11:1) of a 5mM equimolar mixture of **DBA·PF$_6$ & BP23C7**. K_a value calculated from integrations of the complexed and the uncomplexed peaks "1" of **DBA·PF$_6$** is [(1.00/1.56) x 5.00 x 10^{-3}]/[(1-1.00/1.56) x 5.00 x 10^{-3}]^2 = 1.00 x 10^3 M^{-1}.

4. Nominal ESI-MS of a 1:1 mixture of 1-H·PF_6 & BP23C7

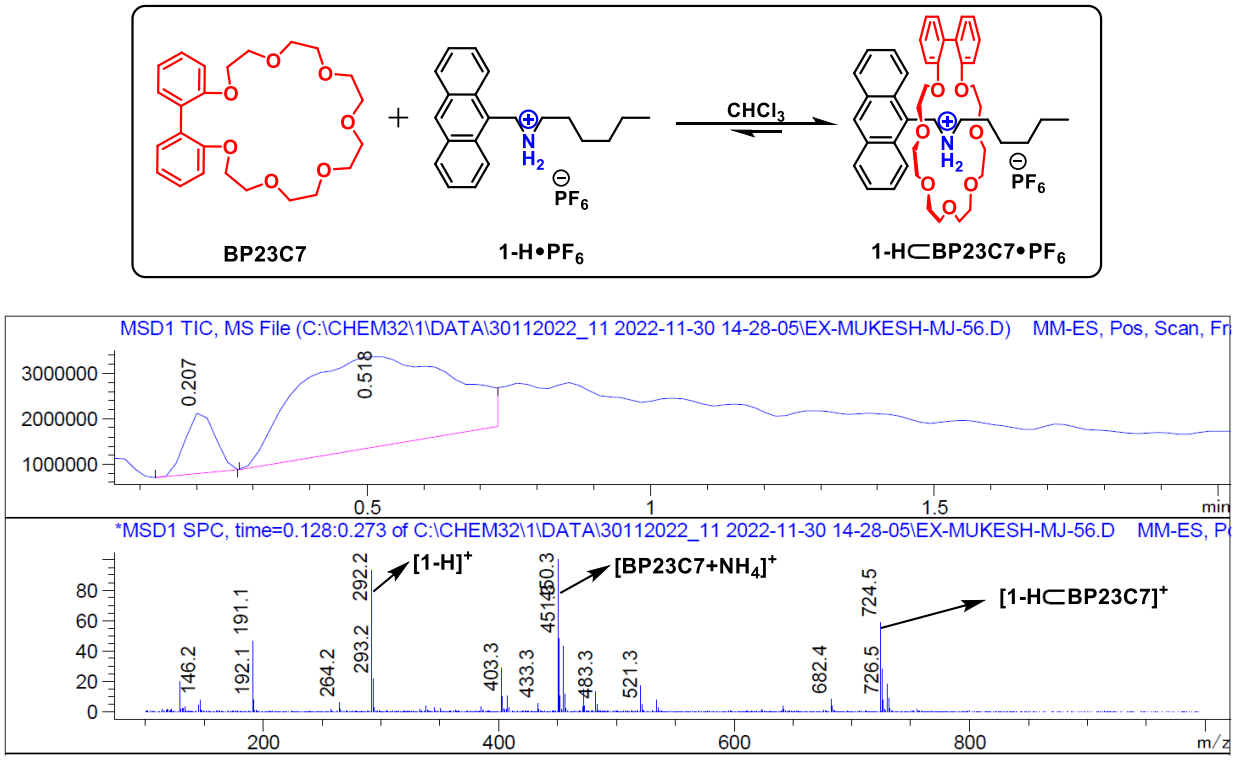

Figure S3. ESI mass spectrum of the equimolar mixture of **1-H·PF_6 & BP23C7** displayed base peak at *m/z* = 724.5 $[M\text{-}PF_6]^+$, where "M" corresponds to the pseudo[2]rotaxane species **1-H⊂BP23C7·PF_6**.

5. ^{1}H NMR spectrum of a 1:1 mixture of 1-H·PF$_6$ & BP23C7

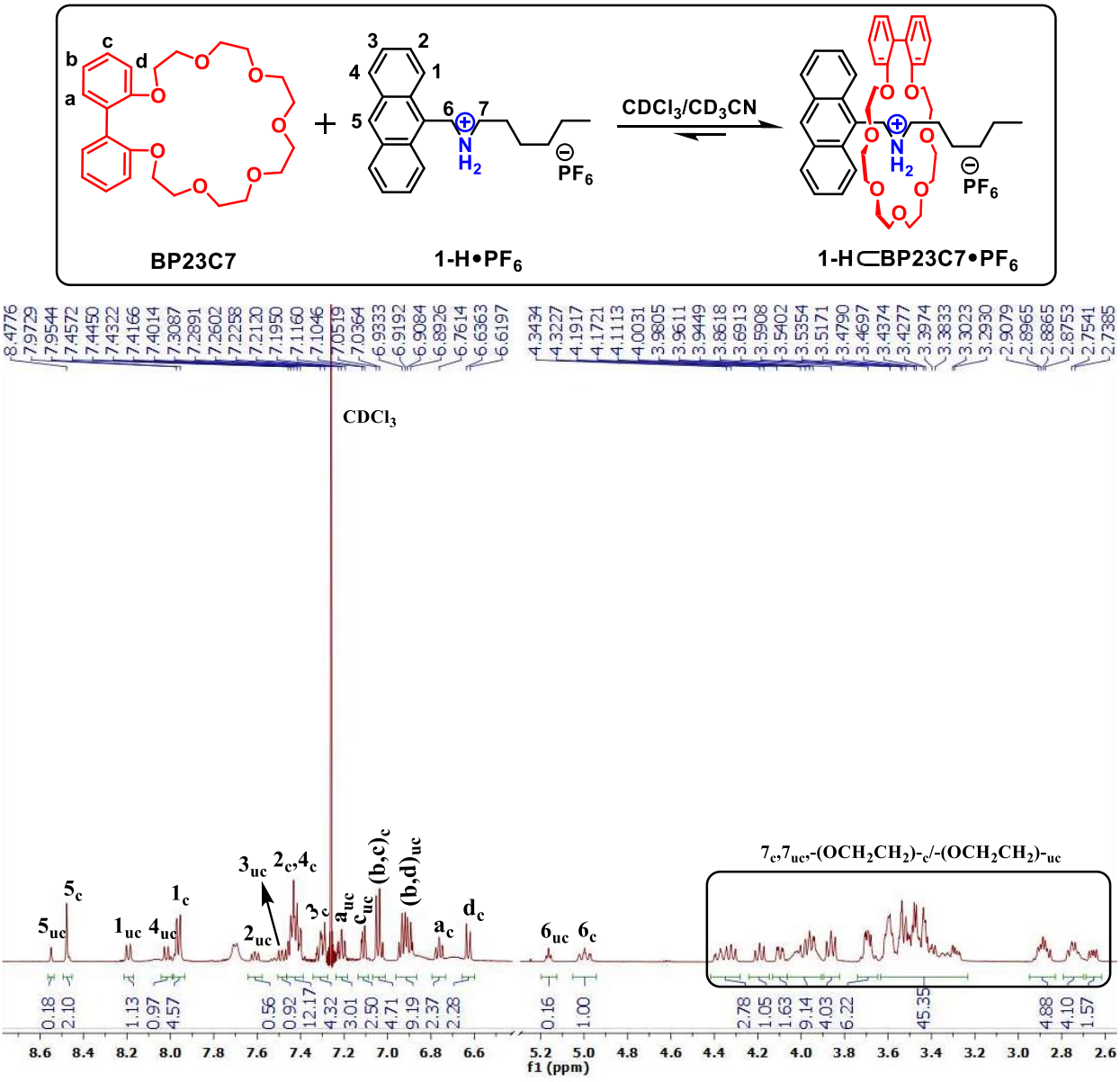

Figure S4. ^{1}H NMR spectrum (500 MHz, $CDCl_3/CD_3CN$ = 11:1) of a 5mM equimolar mixture of **1-H·PF$_6$ & BP23C7**. K_a value calculated from integrations of the complexed and the uncomplexed peaks "6" of **1-H·PF$_6$** is [(1.00/1.16) x 5.00 x 10^{-3}]/[(1-1.00/1.16) x 5.00 x 10^{-3}]^2 = 9.0 x 10^3 M^{-1}.

6. Optical data of the mixture of 1-H·PF$_6$ & BP23C7

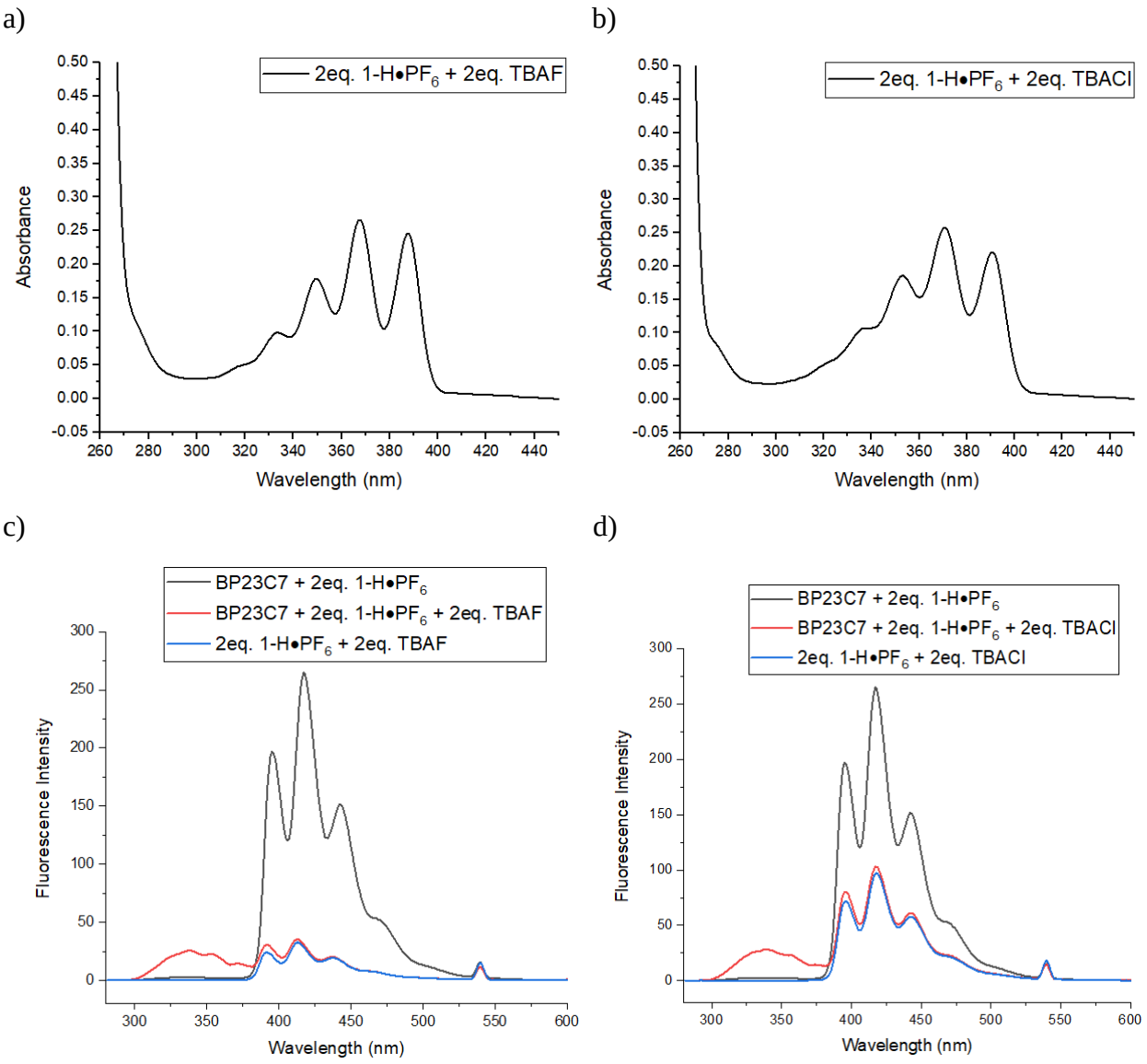

Figure S5. Absorption spectra (CH_2Cl_2, 298 K) of a) 2eq. **1-H·PF$_6$** (4 x 10^{-5} M^{-1}) + 2eq. **TBAF**; and b) 2eq. **1-H·PF$_6$** (4 x 10^{-5} M^{-1}) + 2eq. **TBACl**.

Fluorescence spectra (CH_2Cl_2, λ_{exc} = 270 nm, 298 K) of c) **BP23C7** (2 x 10^{-5} M^{-1}) + 2eq. **1-H·PF$_6$** (black), **BP23C7** + 2eq. **1-H·PF$_6$** + 2eq. **TBAF** (red), 2eq. **1-H·PF$_6$** + 2eq. **TBAF** (blue); and d) **BP23C7** (2 x 10^{-5} M^{-1}) + 2eq. **1-H·PF$_6$** (black), **BP23C7** + 2eq. **1-H·PF$_6$** + 2eq. **TBACl** (red), 2eq. **1-H·PF$_6$** + 2eq. **TBACl** (blue).

7. Nominal ESI-MS of a 1:1 mixture of 2-H·PF_6 & BP23C7

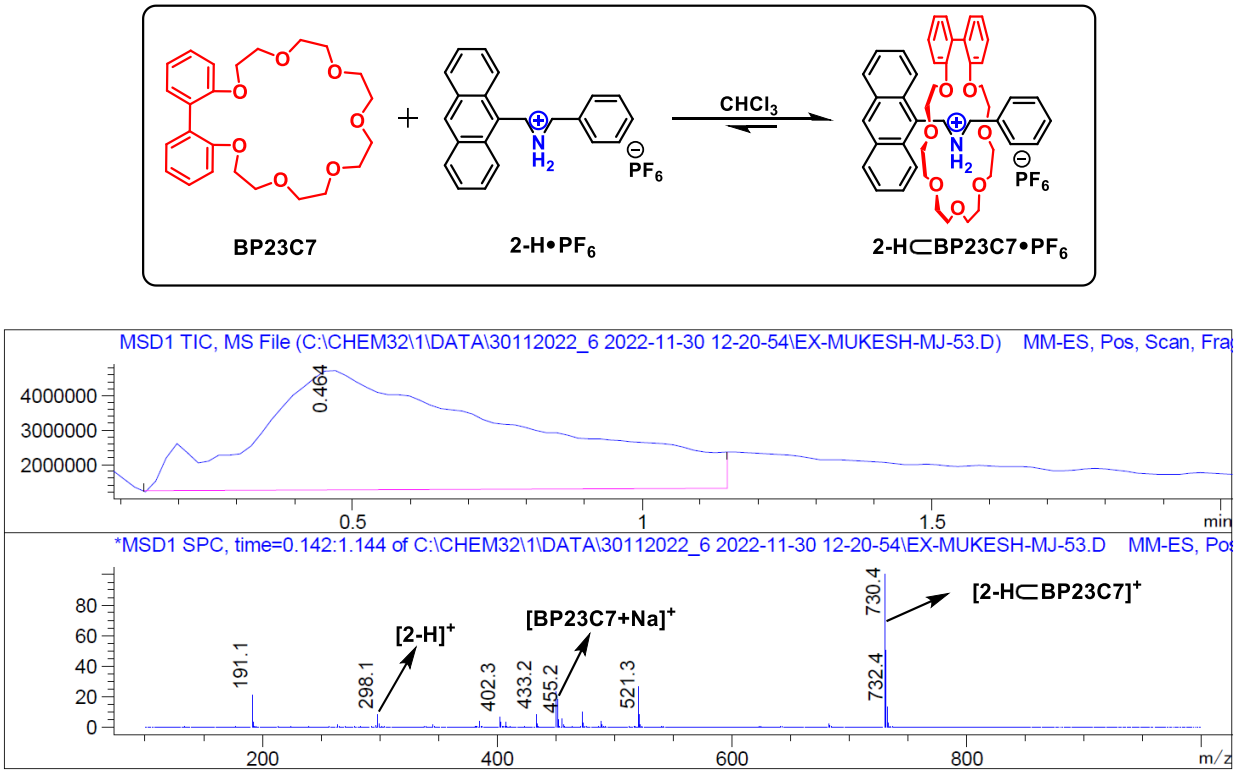

Figure S6. ESI mass spectrum of the equimolar mixture of **2-H·PF_6 & BP23C7** displayed base peak at *m/z* = 730.4 $[M\text{-}PF_6]^+$, where "M" corresponds to the pseudo[2]rotaxane species **2-H⊂BP23C7·PF_6**.

8. ^{1}H NMR spectrum of a 1:1 mixture of 2-H·PF$_6$ & BP23C7

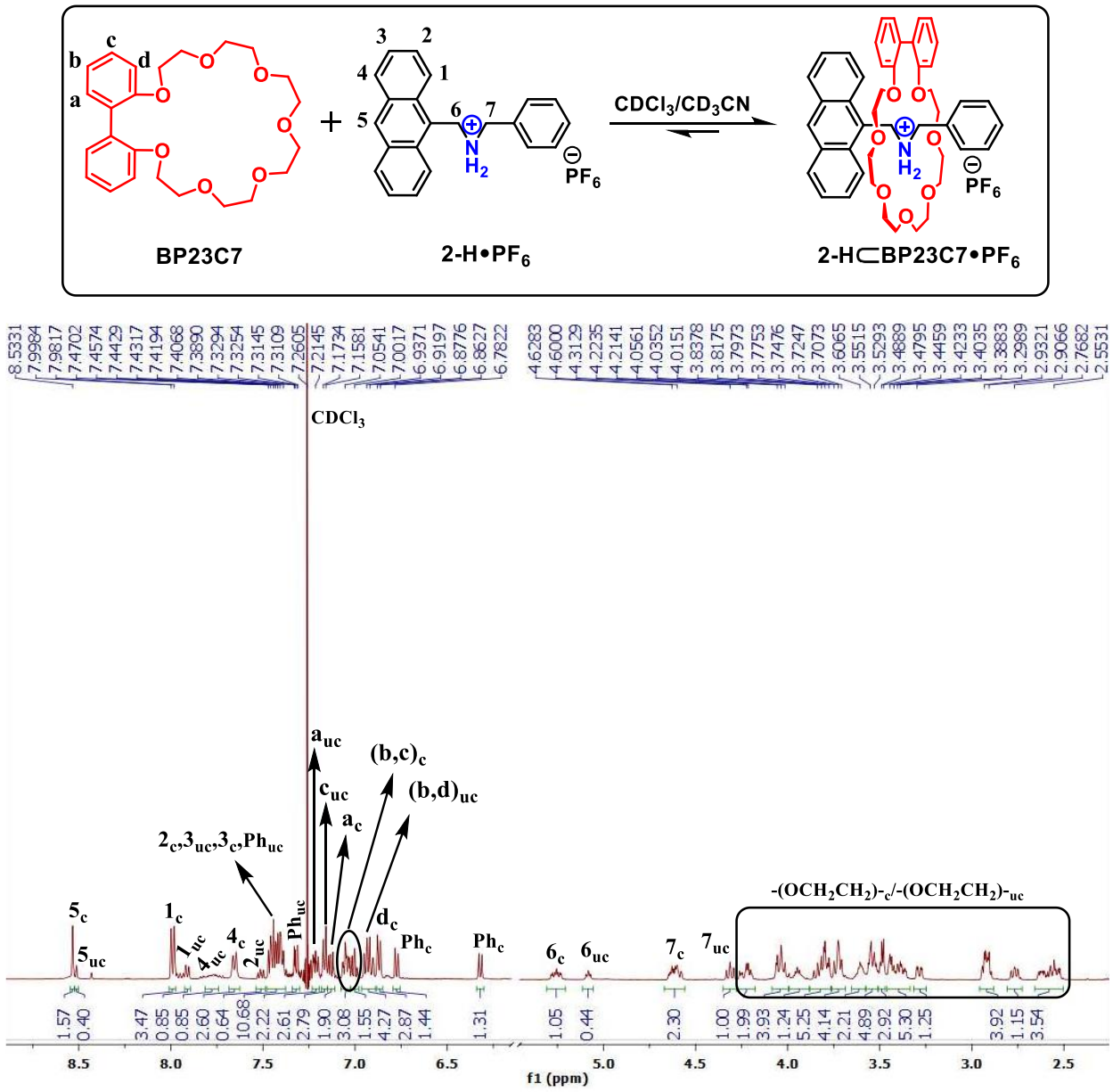

Figure S7. ^{1}H NMR spectrum (500 MHz, $CDCl_3/CD_3CN$ = 11:1) of a 5mM equimolar mixture of **2-H·PF$_6$ & BP23C7**. K_a value calculated from integrations of the complexed and the uncomplexed peaks "6" of **2-H·PF$_6$** is [(1.05/1.49) x 5.00 x 10^{-3}]/[(1-1.05/1.49) x 5.00 x 10^{-3}]^2 = 1.6 x 10^3 M^{-1}.

9. Optical data of the mixture of 2-H·PF$_6$ & BP23C7

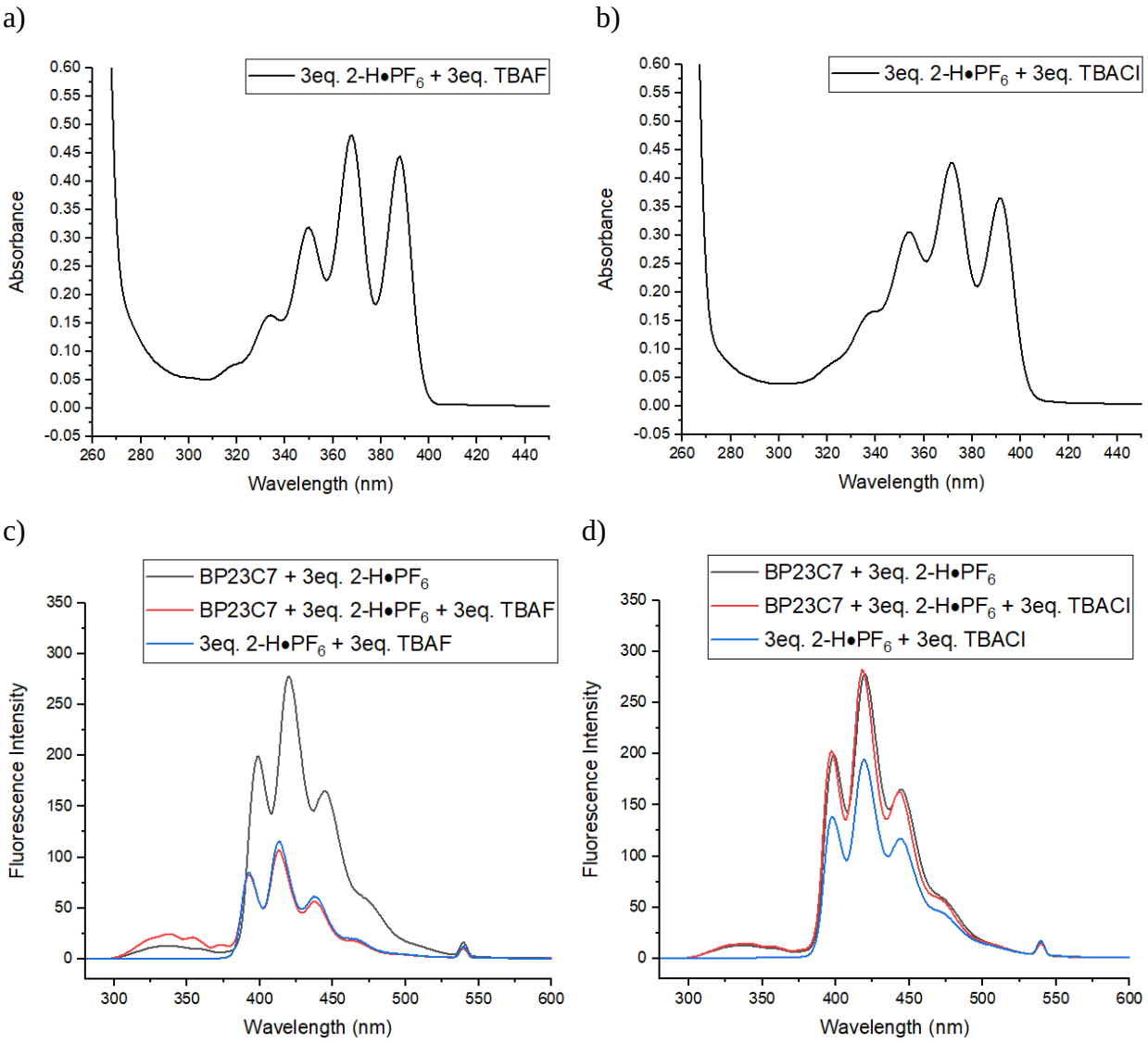

Figure S8. Absorption spectra (CH_2Cl_2, 298 K) of a) 3eq. **2-H·PF$_6$** (6 x 10^{-5} M^{-1}) + 3eq. **TBAF**; and b) 3eq. **2-H·PF$_6$** (6 x 10^{-5} M^{-1}) + 3eq. **TBACl**.

Fluorescence spectra (CH_2Cl_2, λ_{exc} = 270 nm, 298 K) of c) **BP23C7** (2 x 10^{-5} M^{-1}) + 3eq. **2-H·PF$_6$** (black), **BP23C7** + 3eq. **2-H·PF$_6$** + 3eq. **TBAF** (red), 3eq. **2-H·PF$_6$** + 3eq. **TBAF** (blue); and d) **BP23C7** (2 x 10^{-5} M^{-1}) + 3eq. **2-H·PF$_6$** (black), **BP23C7** + 3eq. **2-H·PF$_6$** + 3eq. **TBACl** (red), 3eq. **2-H·PF$_6$** + 3eq. **TBACl** (blue).

10. Fluorescence titration of BP23C7 with 1-H·PF_6 & 1-H·Cl

a)

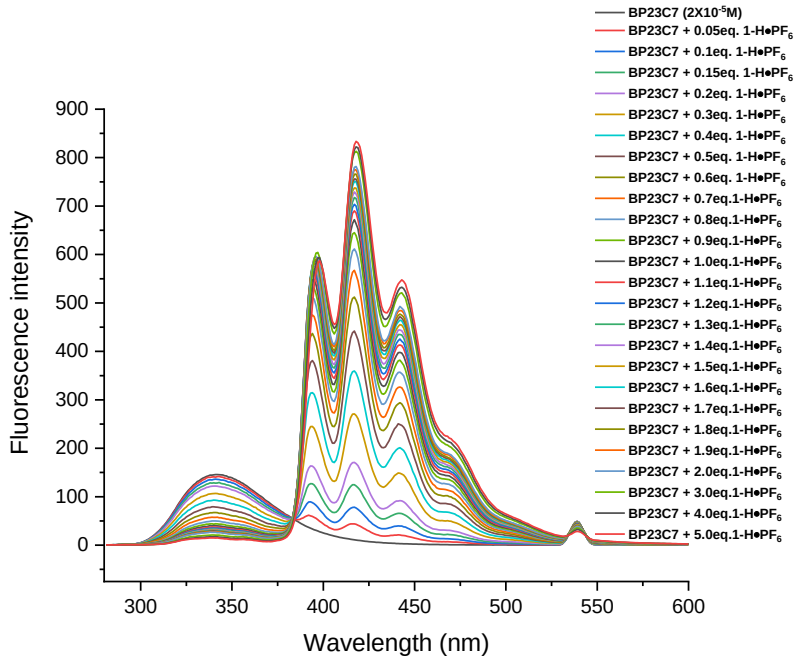

b)

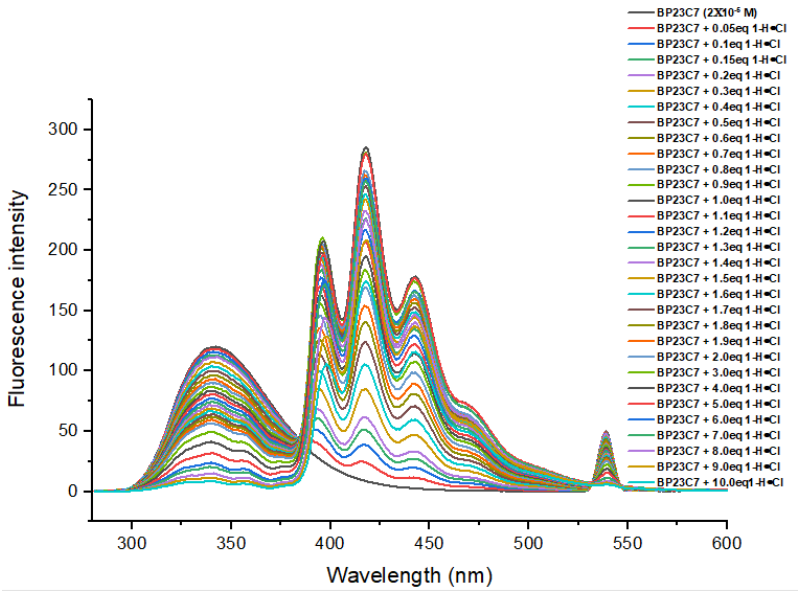

Figure S9. Fluorescence titration experiment of BP23C7 (2 x 10^{-5} M) with a) **1-H·PF_6** and b**) 1-H·Cl**.

11. Fluorescence titration of BP23C7 with 2-H·PF_6

a)

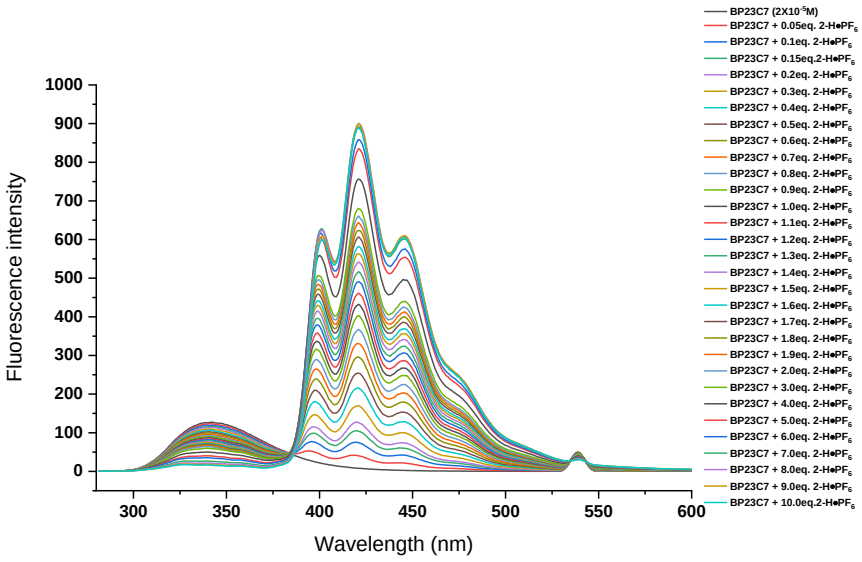

b) **c)**

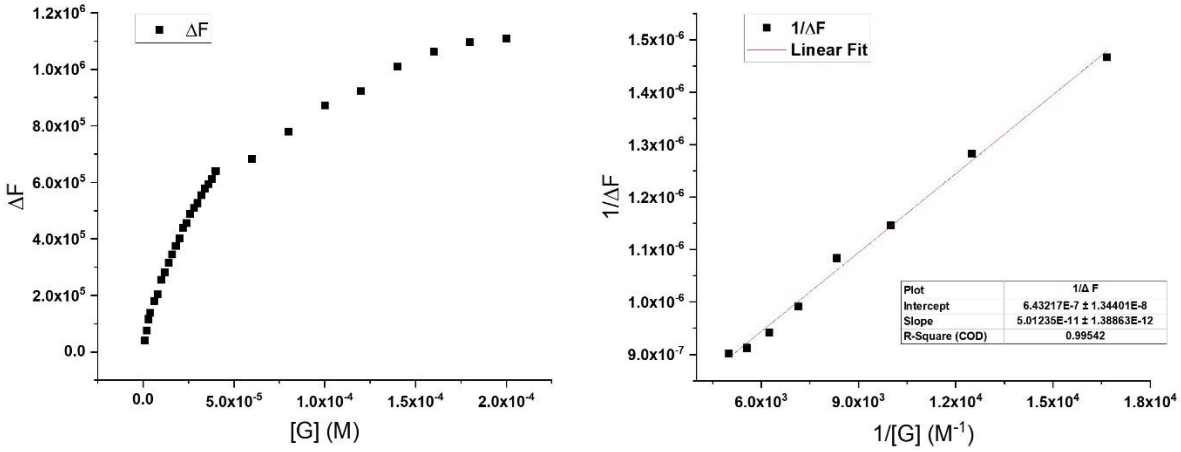

Figure S10. a) Fluorescence titration experiment of BP23C7 (2 x 10^{-5} M) with **2-H·PF_6**, b) Plot of change in fluorescence quenching of BP23C7 with concentration of **2-H·PF_6**; c) Benesi-Hildebrand plot from fluorescence titration data of (a), K_a = Intercept/Slope = (1.283 ± 0.008) x 10^4 M^{-1}.

12. 2D NOESY NMR spectrum of the [3]Rotaxane 10-H_2·2PF_6

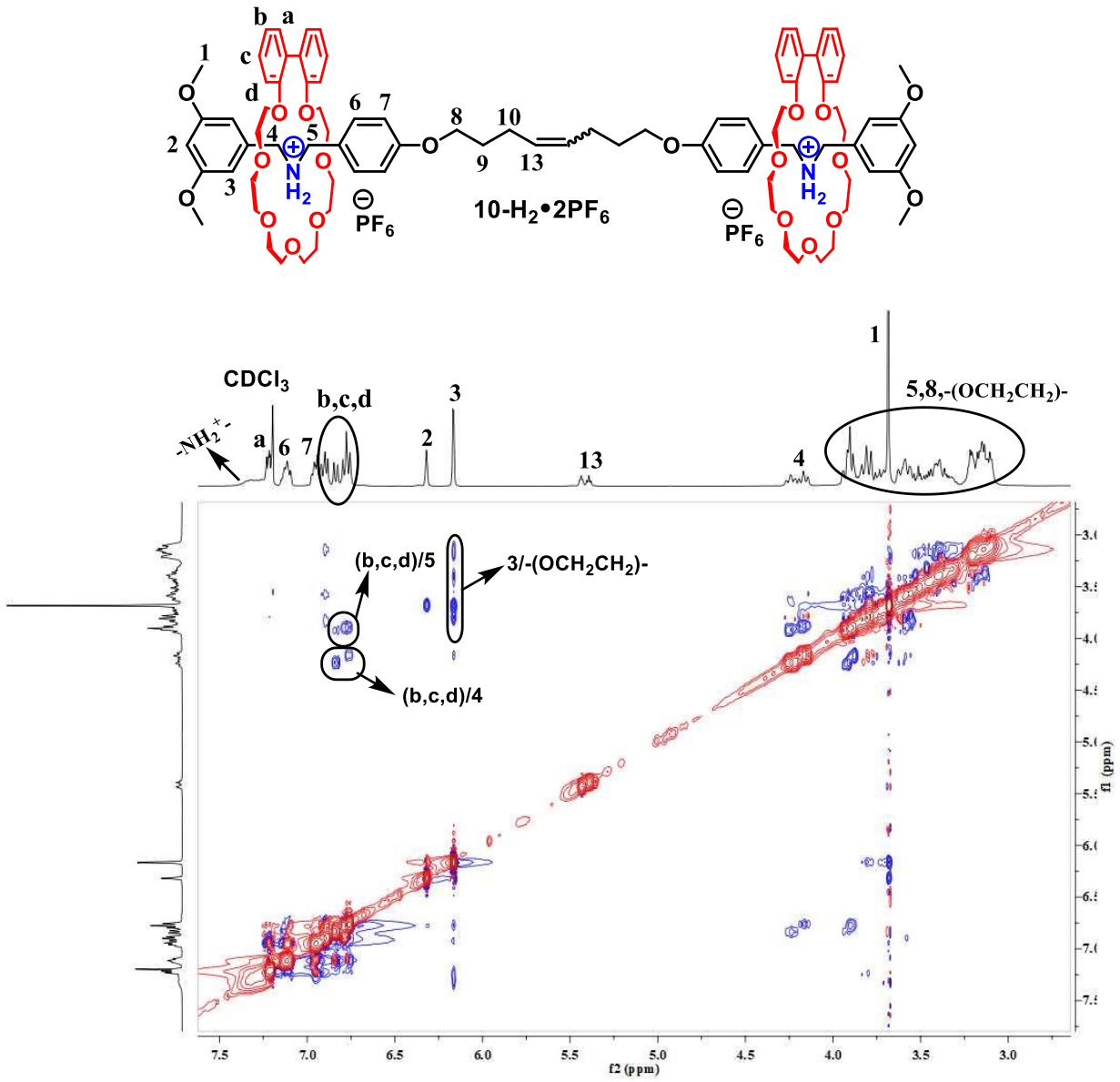

Figure S11. ^{1}H-^{1}H NOESY NMR (400 MHz, $CDCl_3$) of **10-H_2·2PF_6**. In this case, a strong correlation between (-OCH_2CH_2-) protons of **BP23C7** with the aromatic protons H_3 of the stopper group is seen. Moreover, strong NOE cross peaks between **BP23C7** aromatic protons H_b, H_c, H_d and the benzylic protons H_4 and H_5 of the axle corroborates the interlocking geometry.

13. HR ESI-MS spectrum of the [3]Rotaxane 10-H_2·2PF_6

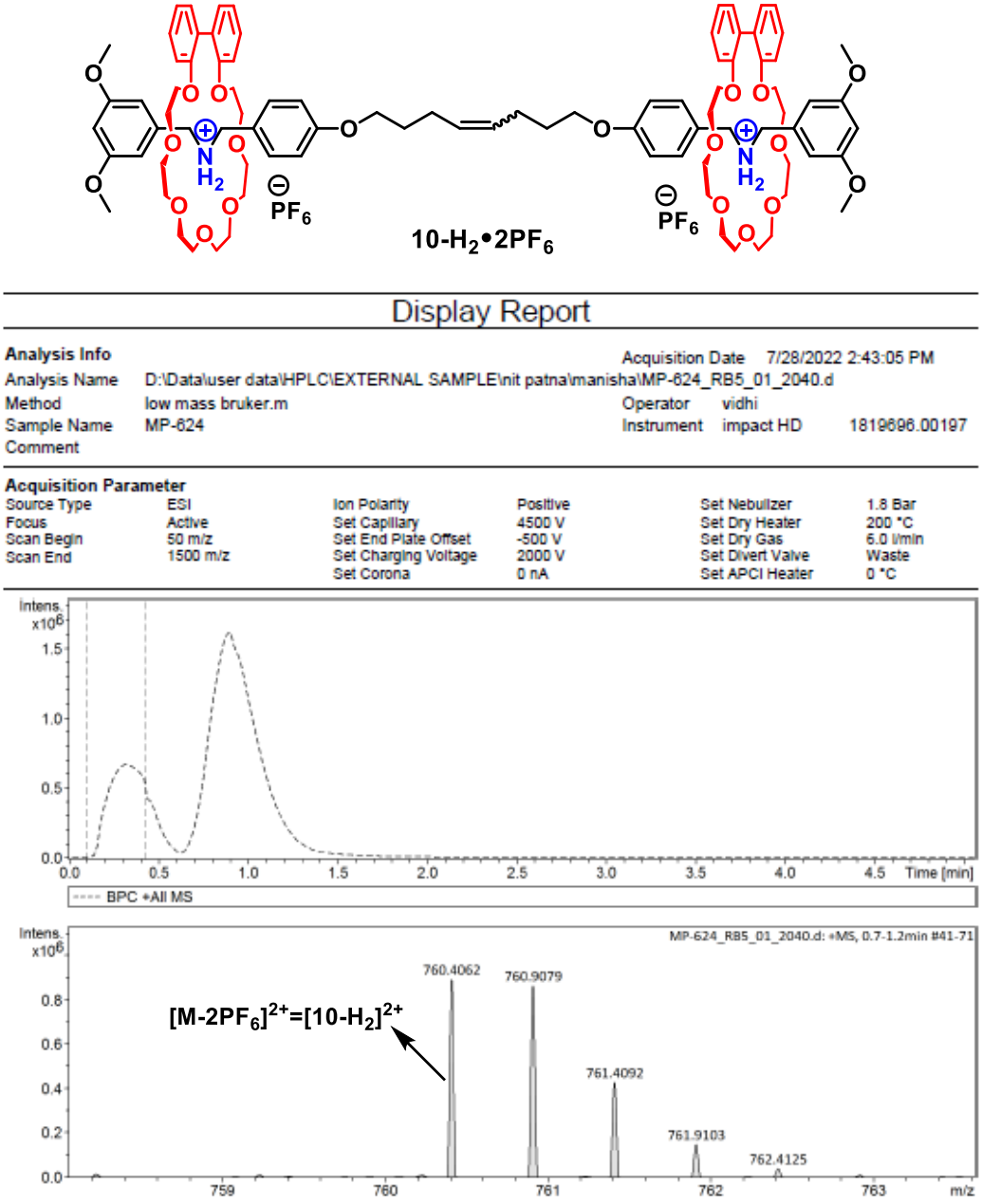

Figure S12. HR ESI-MS spectrum of the [3]rotaxane **10-H_2·2PF_6**. Peak at *m/z* = 760.4062 corresponds to $[M\text{-}2PF_6]^{2+}$ species. Isotopic distribution aptly reaffirms the effective species as the dicationic species, **$[10\text{-}H_2]^{2+}$**. HR MS (ESI): *m/z* Calcd for $C_{88}H_{116}N_2O_{20}^{2+}$ $(M\text{-}2PF_6)^{2+}$: 760.4055 (100%), 760.9072 (95.2%).

14. 2D NOESY NMR spectrum of the [3]Rotaxane 11-H_2·2PF_6

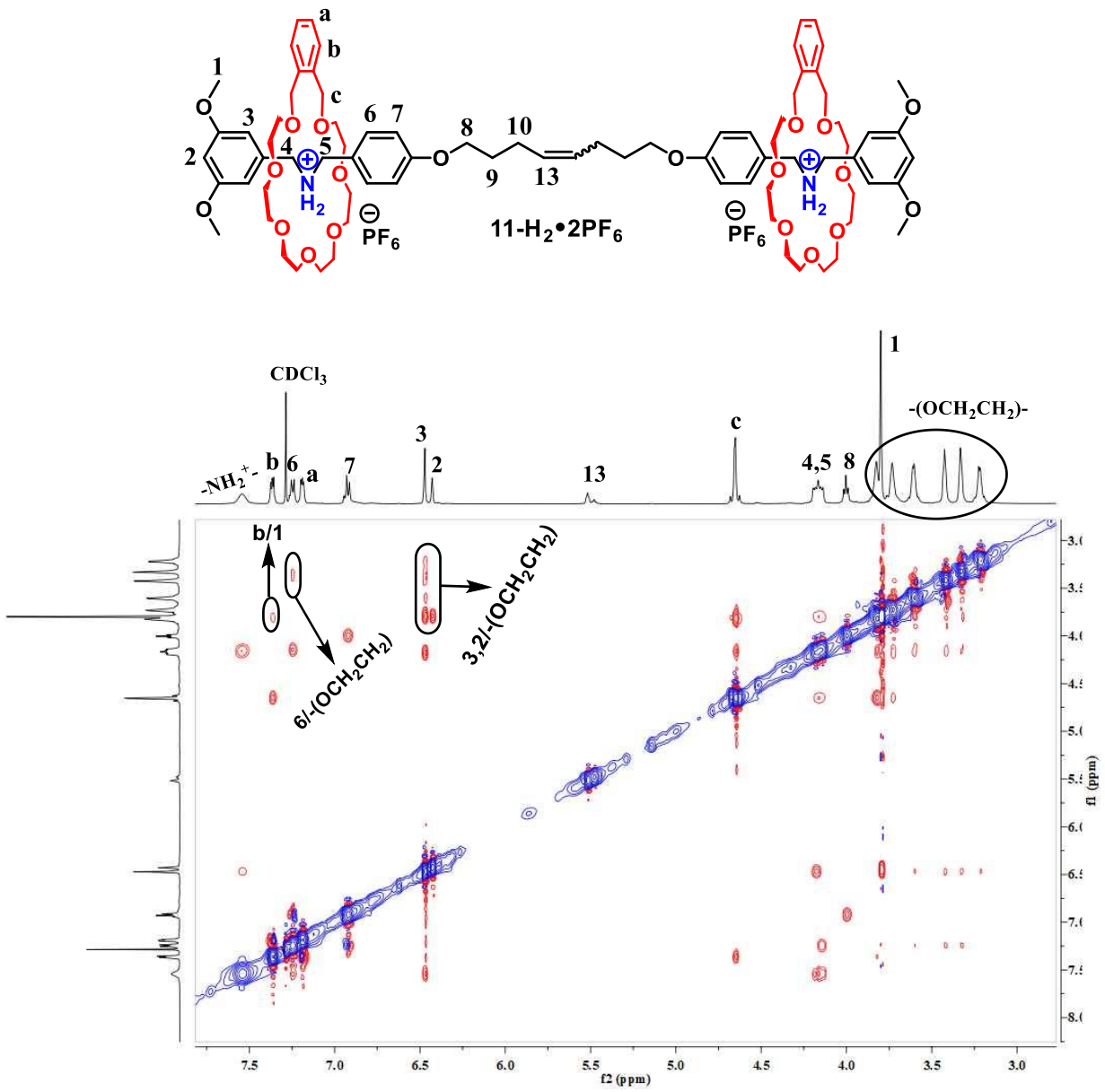

Figure S13. ^{1}H-^{1}H NOESY NMR (400 MHz, $CDCl_3$) of **11-H_2·2PF_6**. In this case, strong correlations between (-OCH_2CH_2-) protons of **X23C7** with the aromatic protons H_2/H_3/H_6 of the axle are observed. Additional correlations such as "H_b/H_1" unambiguously indicates the interlocked geometry.

15. HR ESI-MS spectrum of the [3]Rotaxane 11-H_2·2PF_6

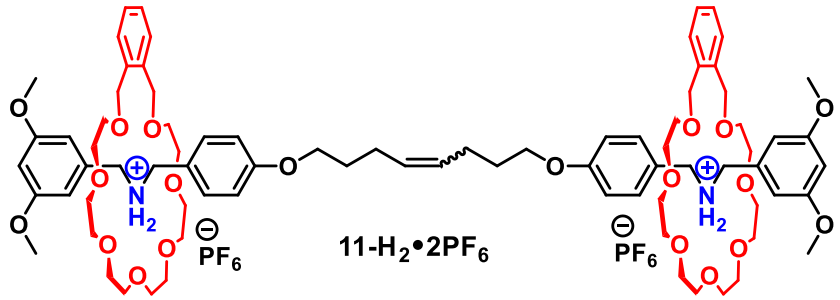

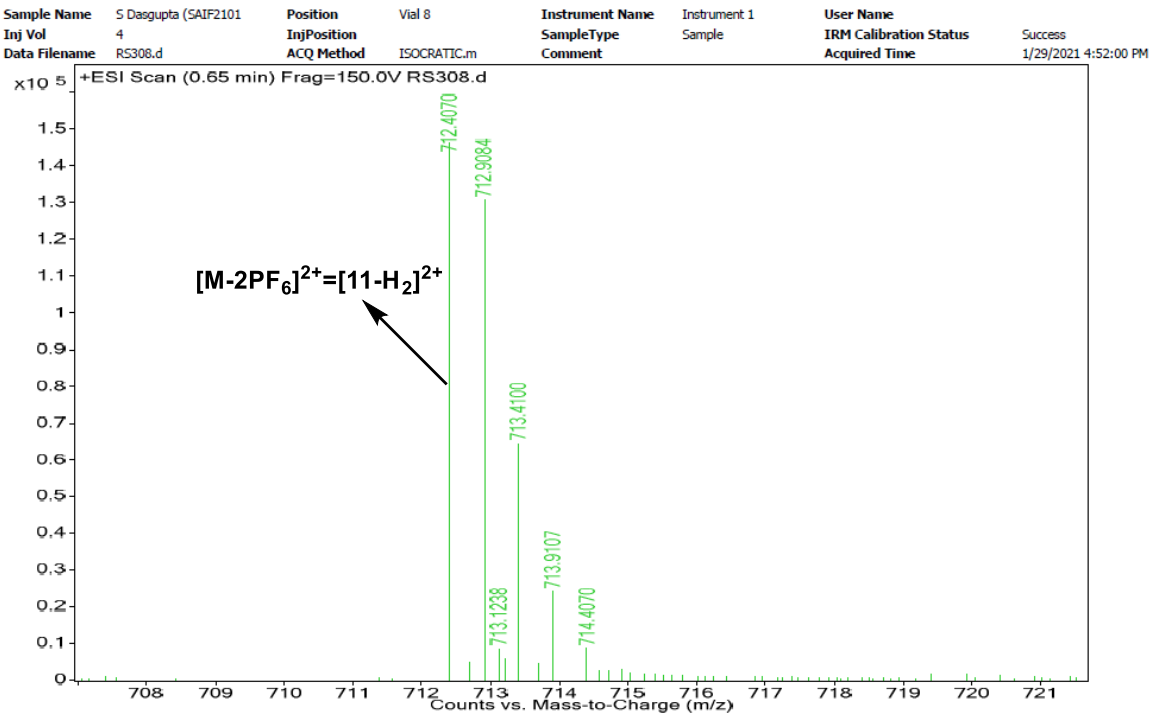

Figure S14. HR ESI-MS spectrum of the [3]rotaxane **11-H_2·2PF_6**. Peak at *m/z* = 712.4070 corresponds to the $[M\text{-}2PF_6]^{2+}$ species. Isotopic distribution clearly suggests the effective species as the dicationic species, **$[11\text{-}H_2]^{2+}$**. HR MS (ESI): *m/z* Calcd for $C_{80}H_{116}N_2O_{20}^{2+}$ $(M\text{-}2PF_6)^{2+}$: 712.4055 (100%), 712.9072 (86.5%).

16. ^{1}H NMR & ^{13}C NMR spectra of all synthesized compounds

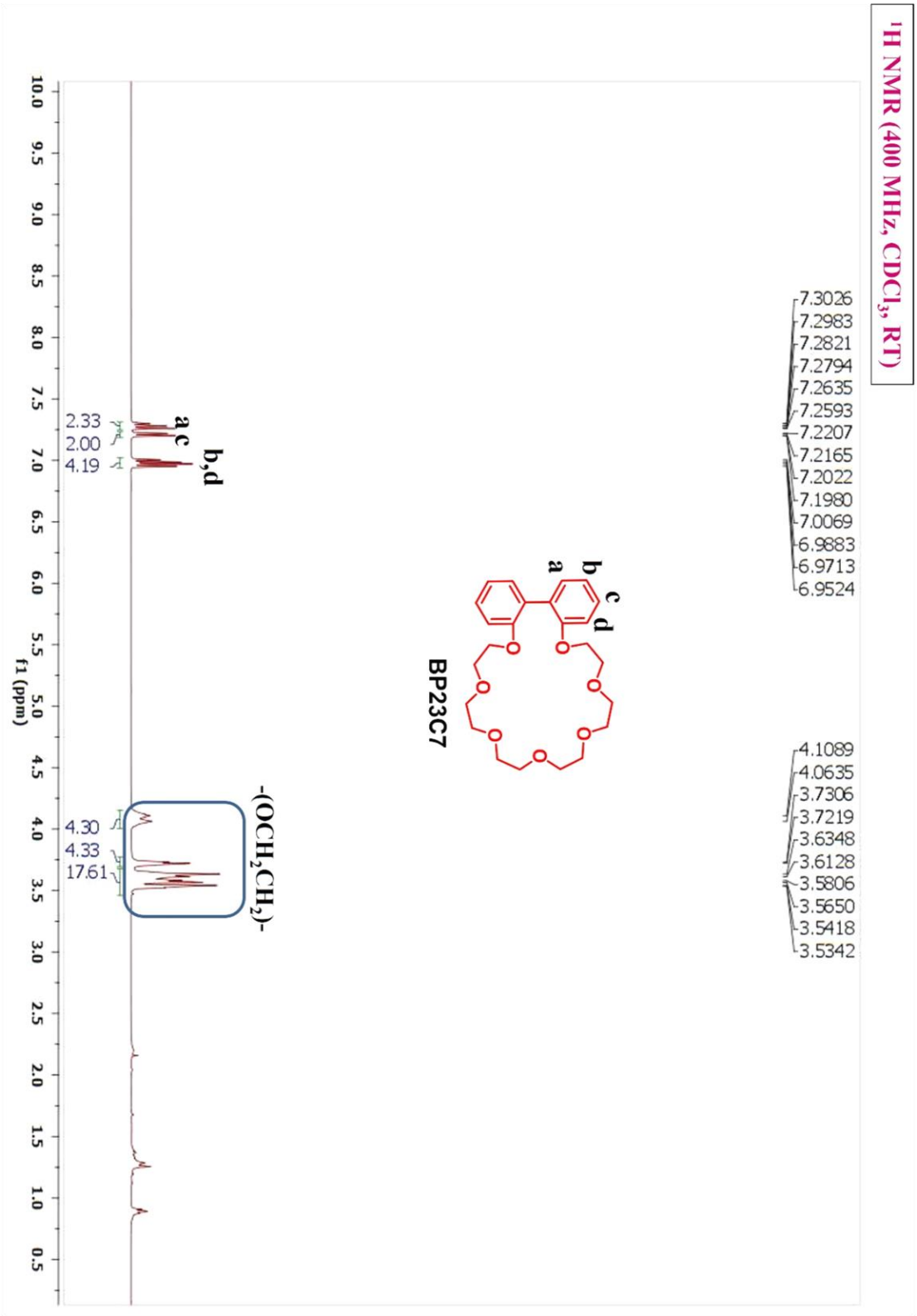

$^{13}C\{^{1}H\}$ NMR (125 MHz, $CDCl_3$, RT)

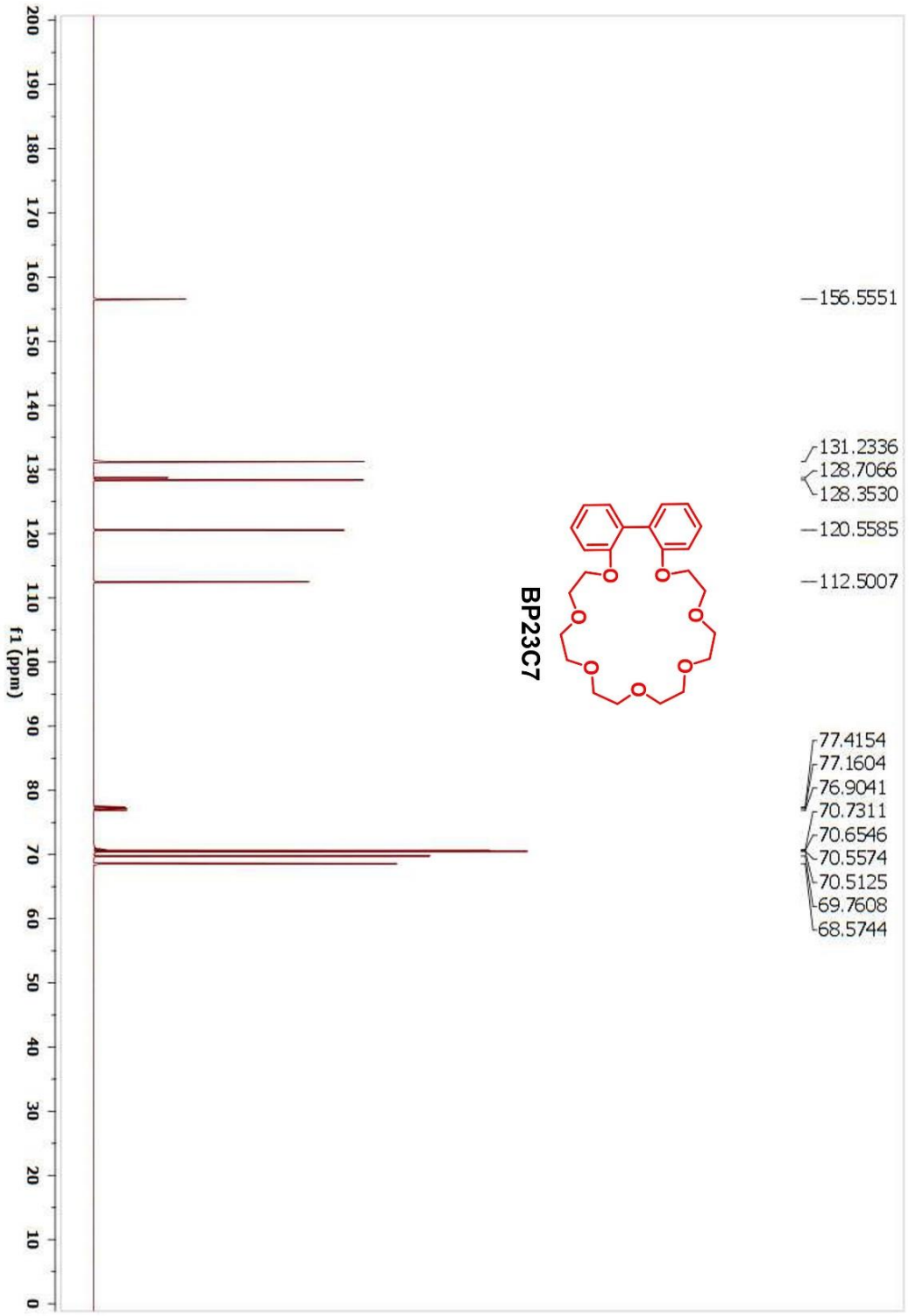

^{1}H NMR (500 MHz, $CDCl_3$, RT)

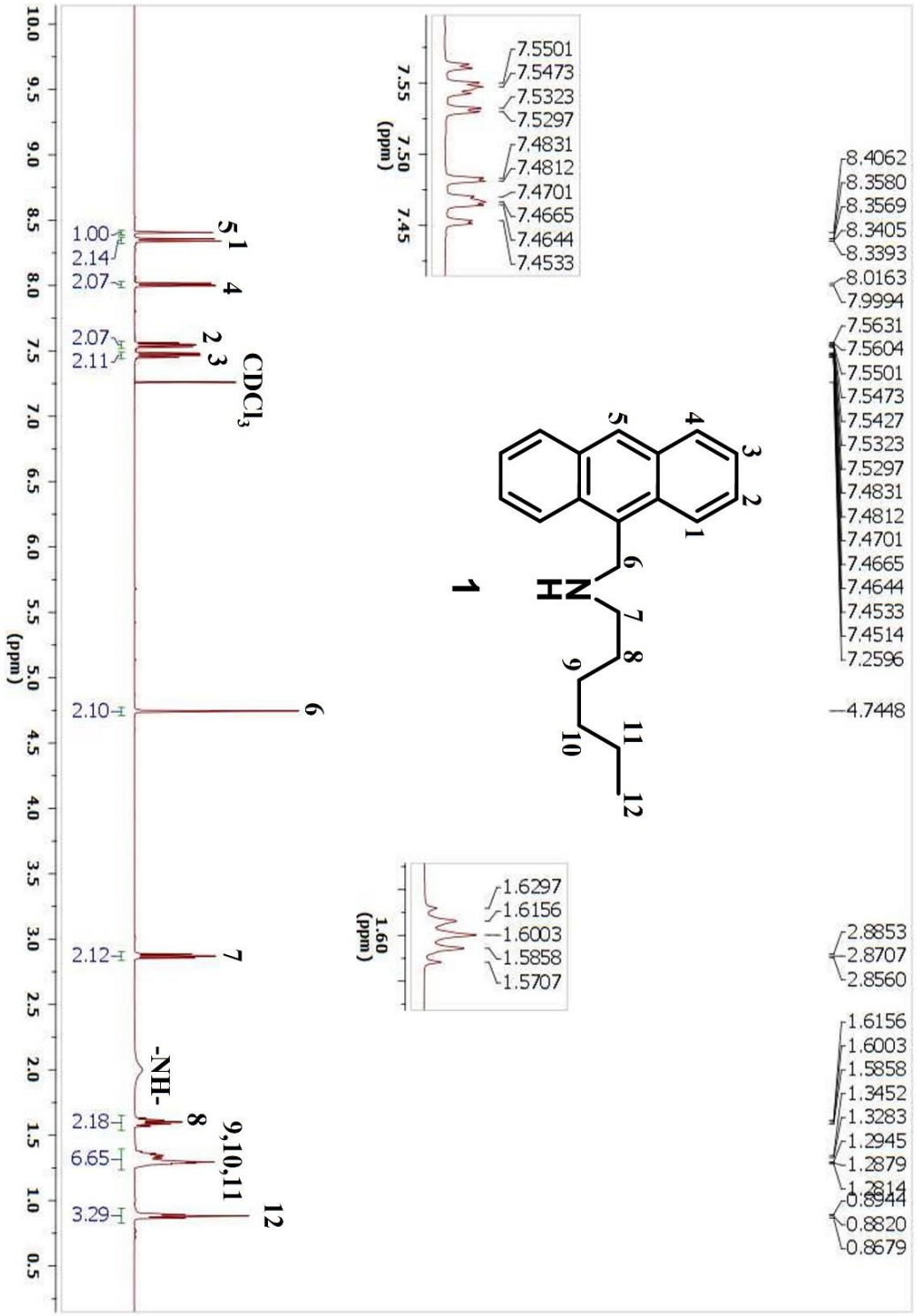

$^{13}C\{^1H\}$ NMR (125 MHz, $CDCl_3$, RT)

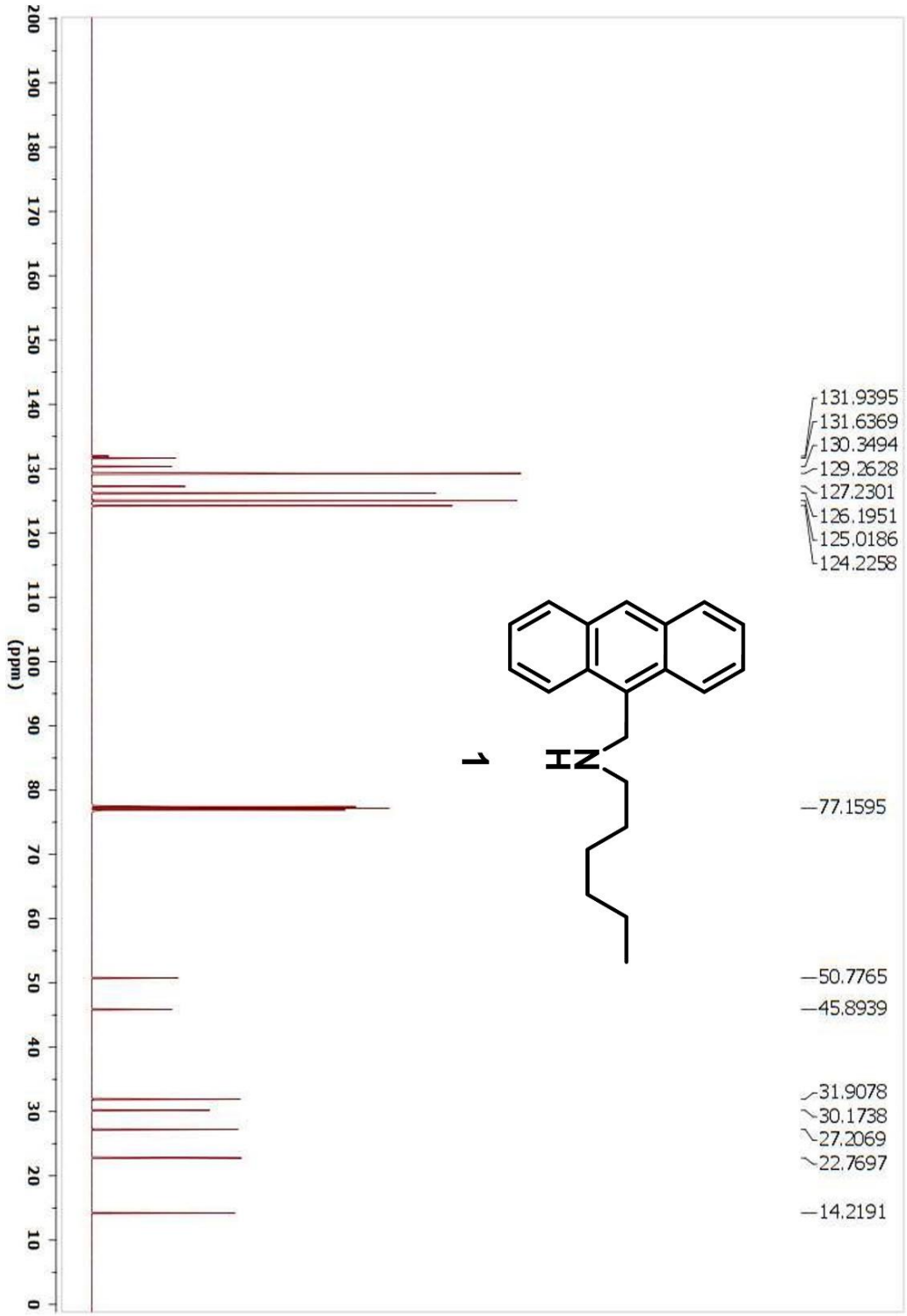

^{1}H NMR (500 MHz, $CDCl_3/CD_3CN$ (11:1), RT)

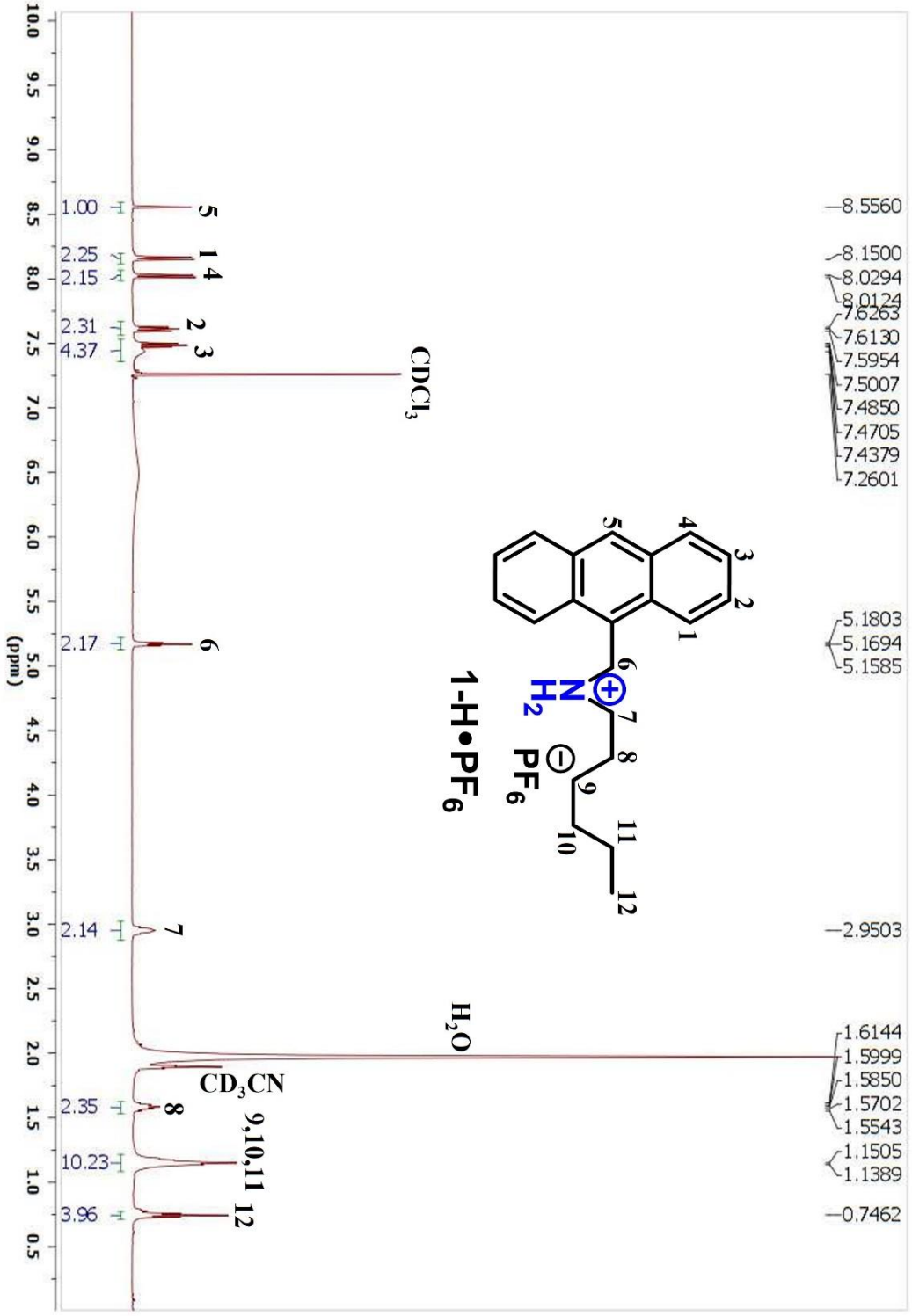

$^{13}C\{^1H\}$ NMR (125 MHz, DMSO-d_6, RT)

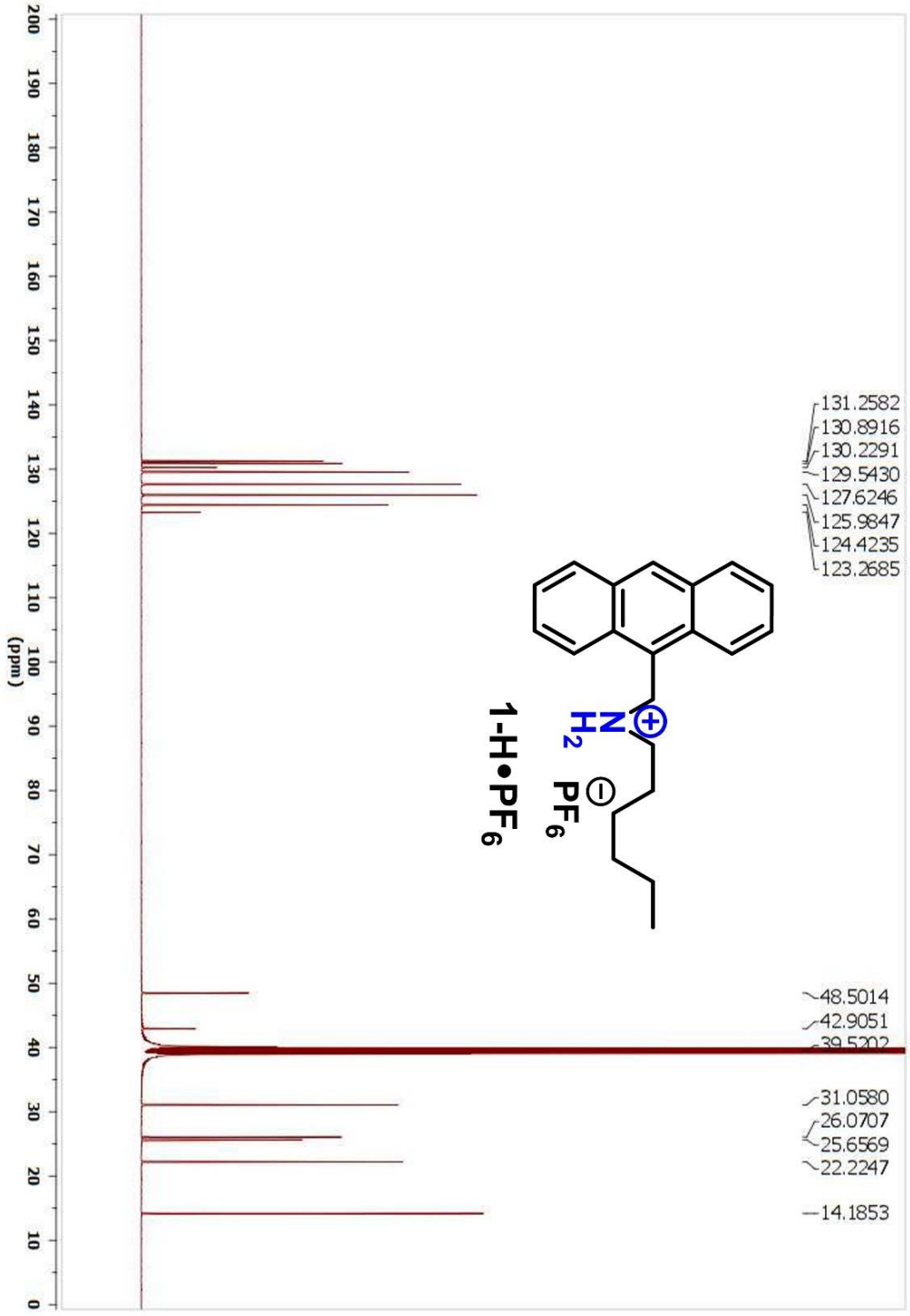

^{1}H NMR (500 MHz, $CDCl_3$, RT)

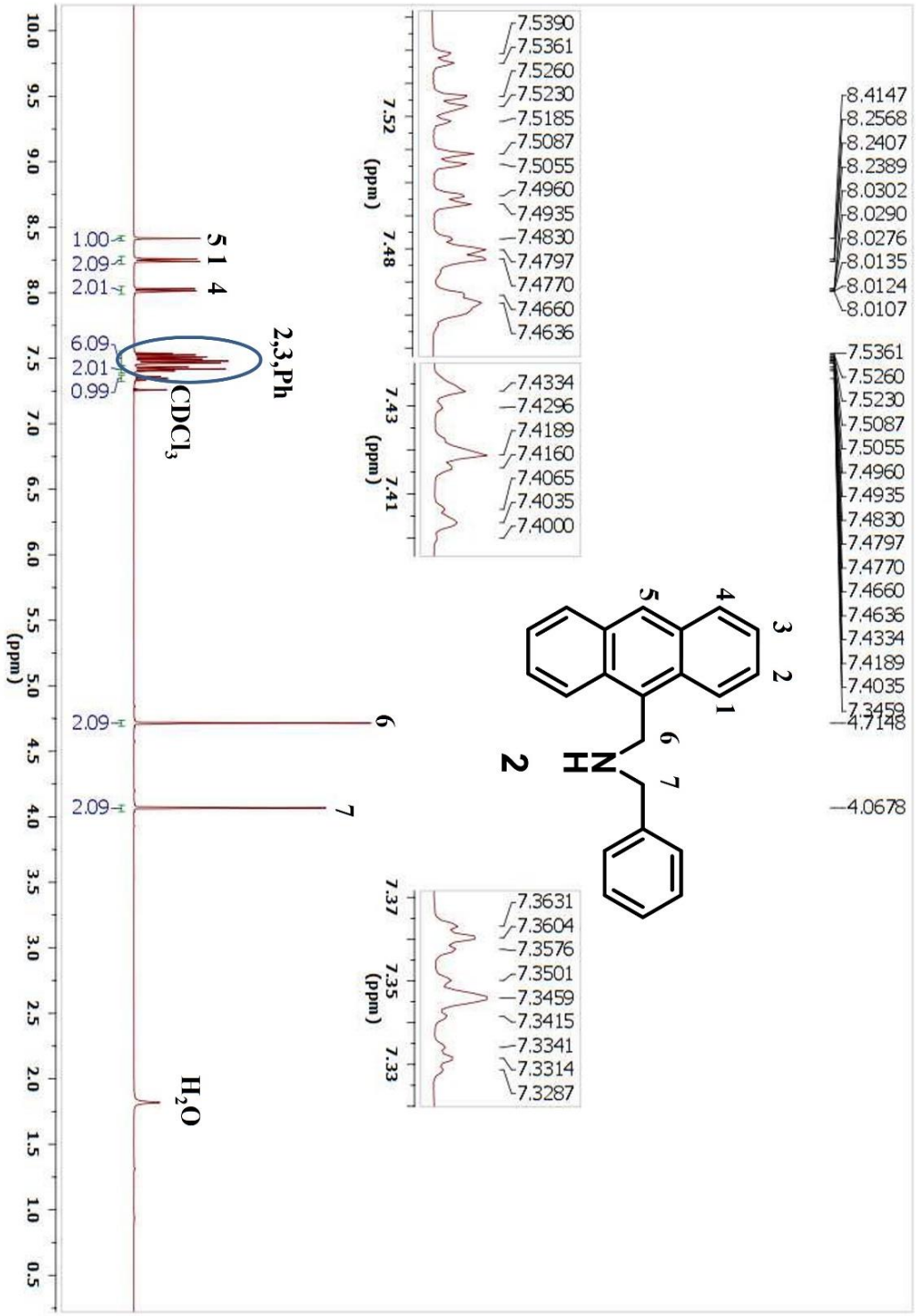

$^{13}C\{^1H\}$ NMR (125 MHz, $CDCl_3$, RT)

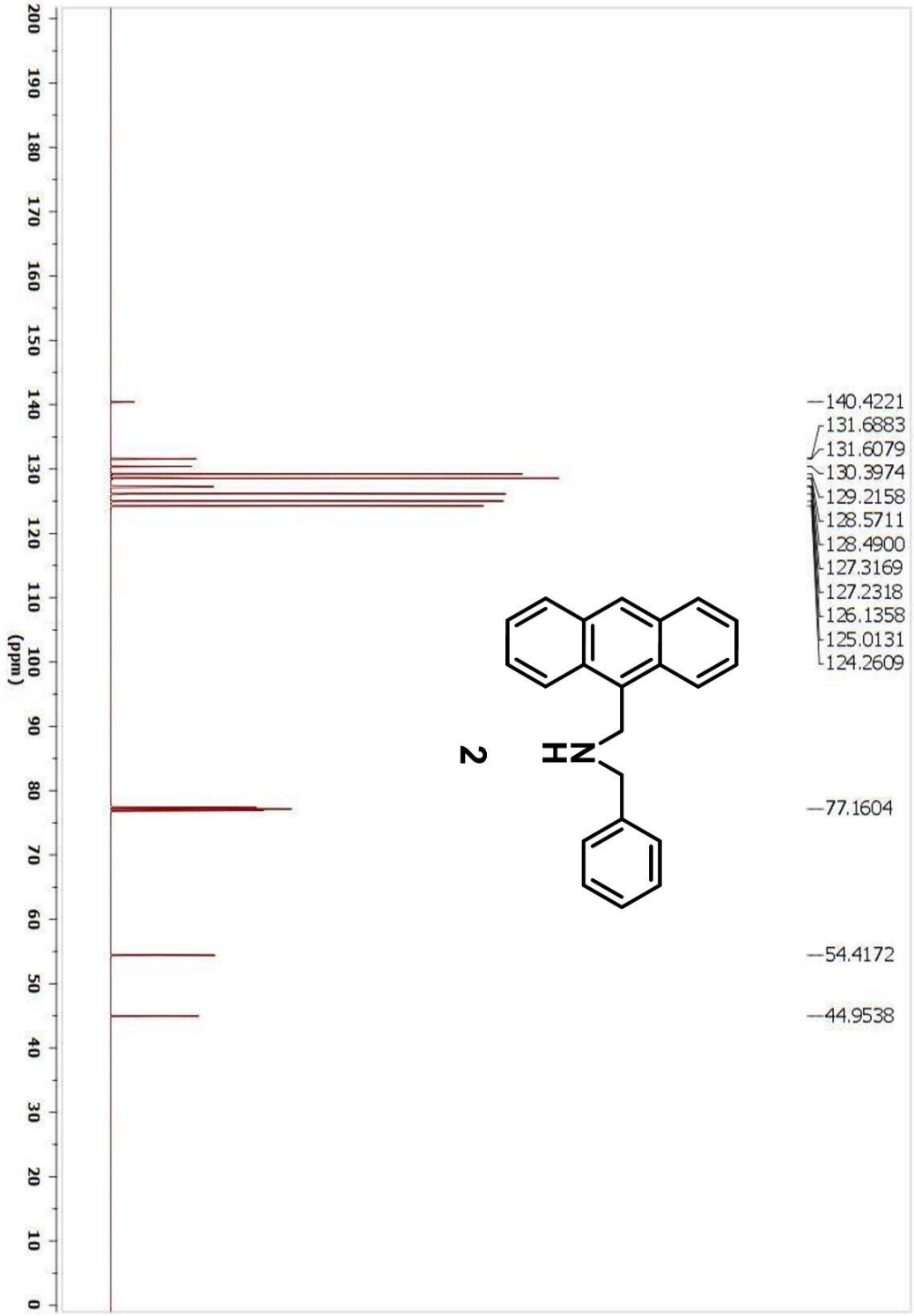

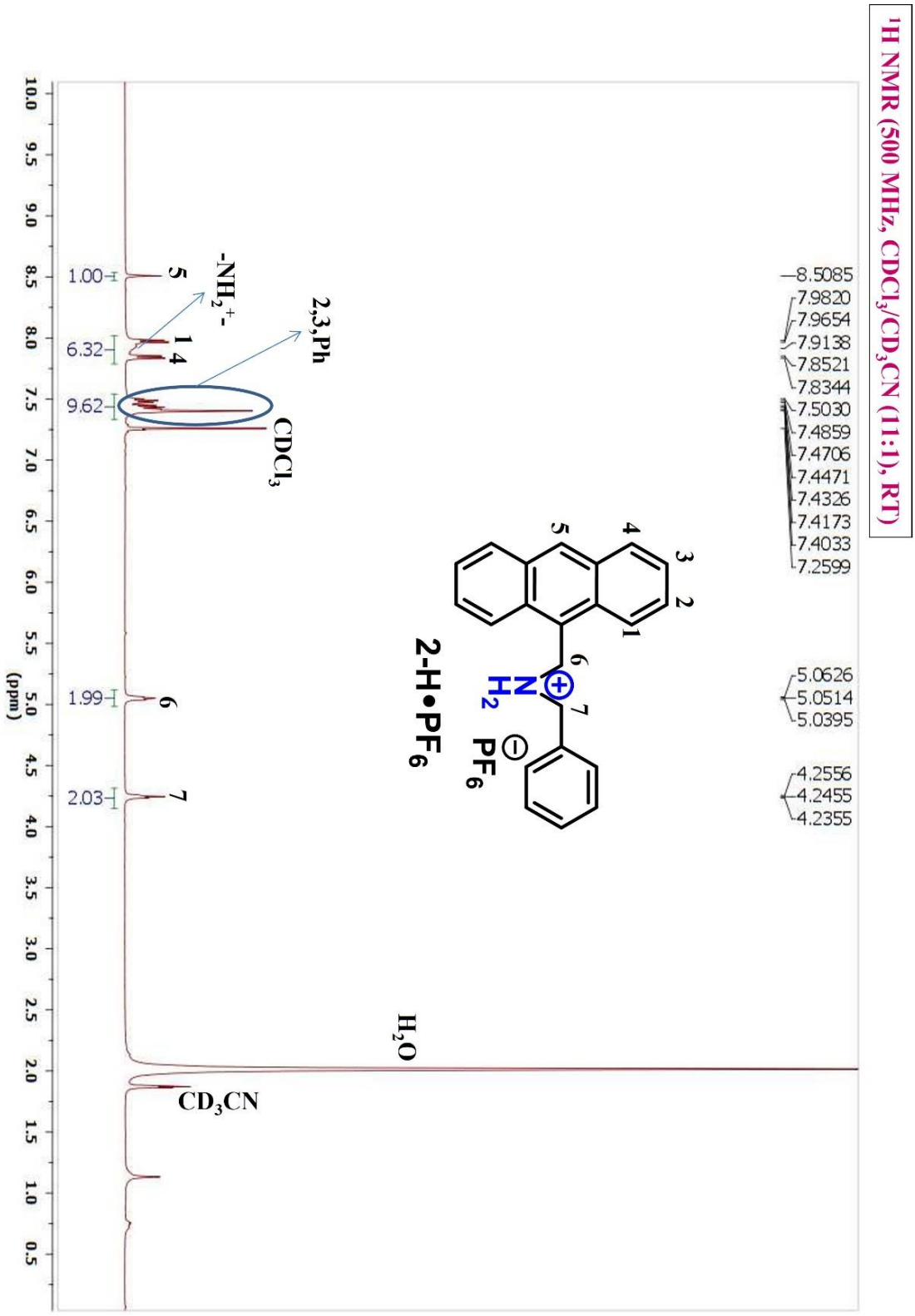
¹H NMR (500 MHz, CDCl3/CD3CN (11:1), RT)
8.5085
7.9820
7.9654
7.9138
7.8521
7.8344
7.5030
7.4859
7.4706
7.4471
7.4326
7.4173
7.4033
7.2599
5.0626
5.0514
5.0395
4.2556
4.2455
4.2355
2-H•PF6
-NH2+-
2,3,Ph
CDCl3
H2O
CD3CN
1.00
6.32
9.62
1.99
2.03
5
1 4
6
7
(ppm)

$^{13}C\{^1H\}$ NMR (125 MHz, DMSO-d_6, RT)

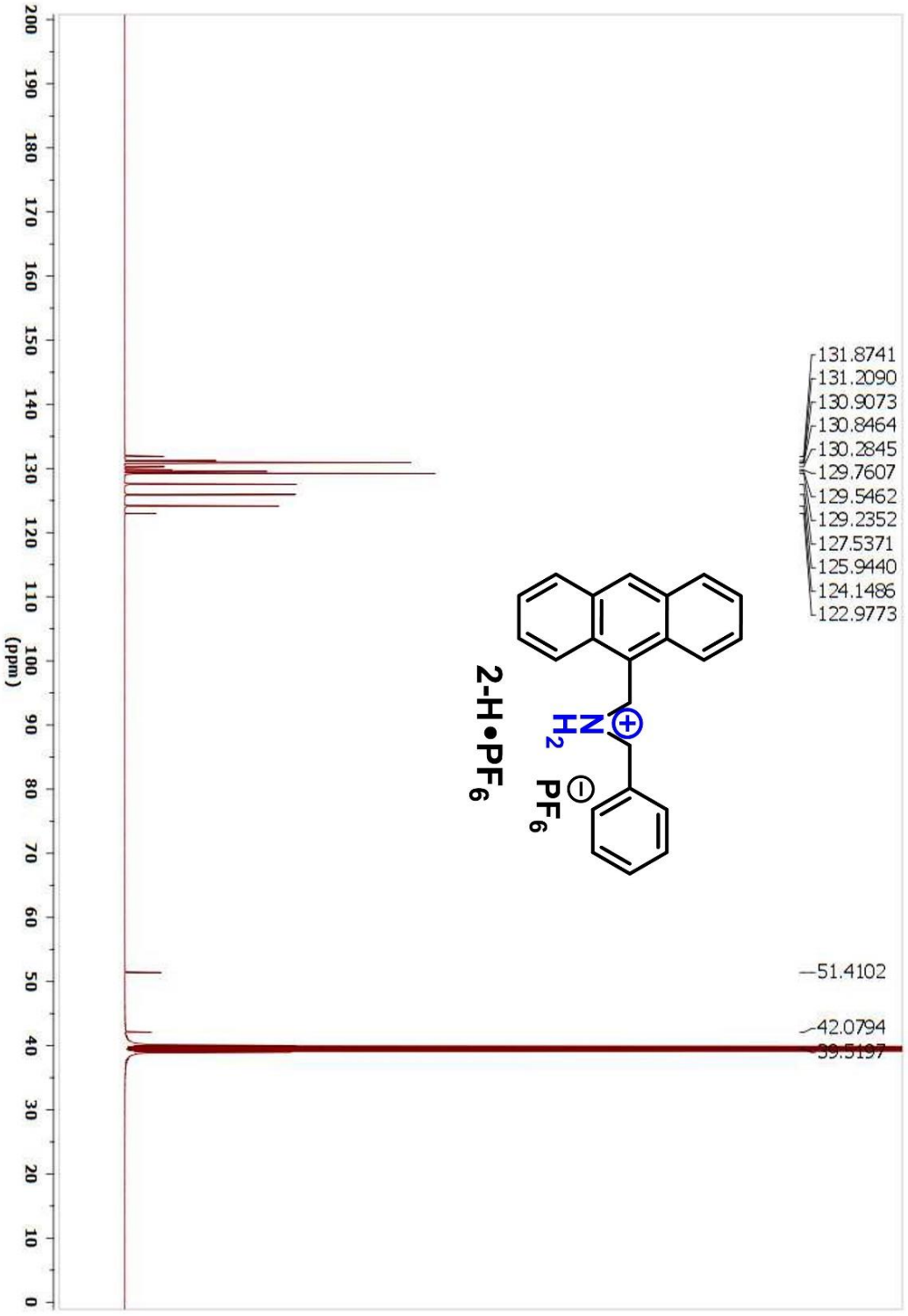

^{1}H NMR (400 MHz, $CDCl_3$, RT)

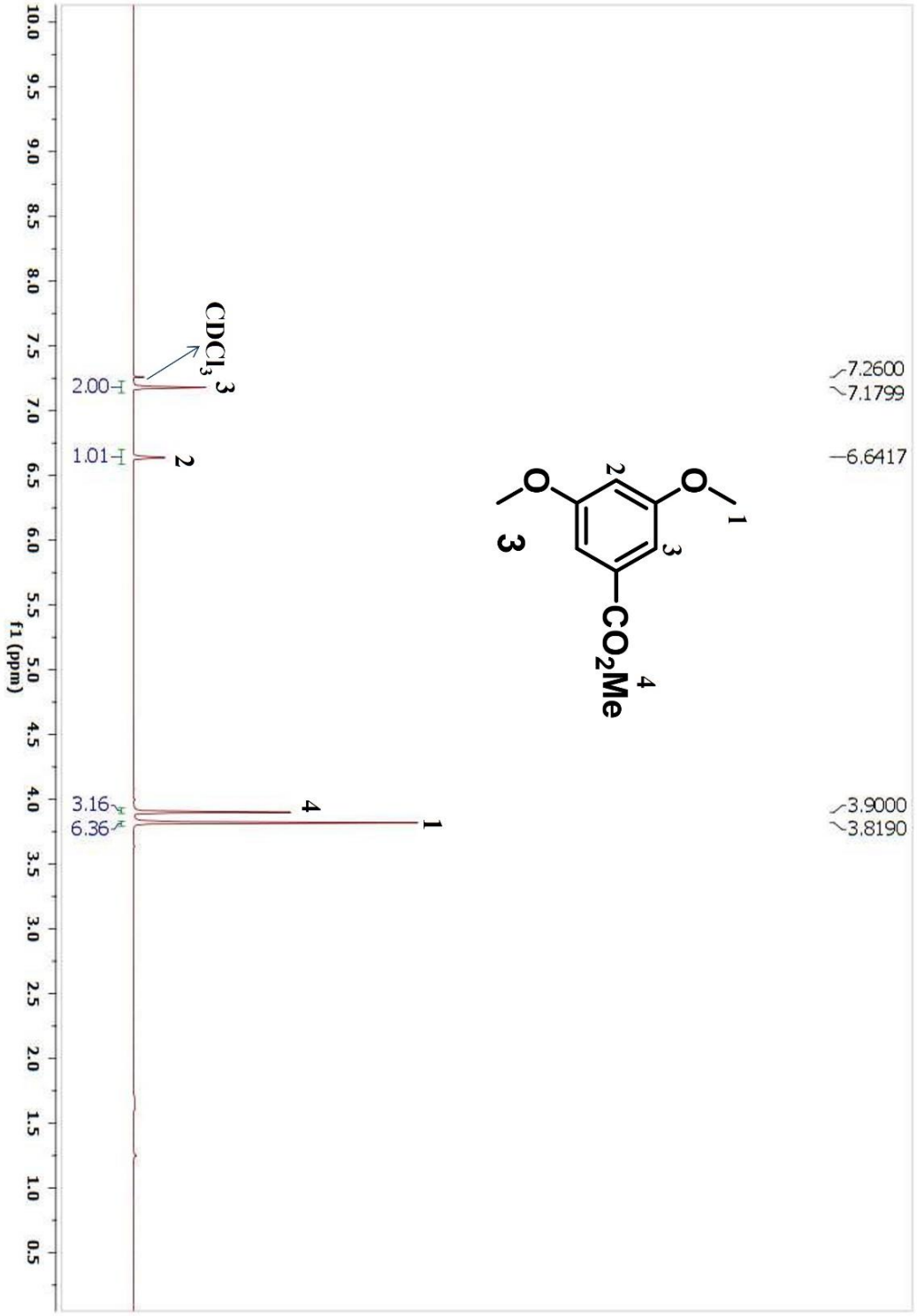

$^{13}C\{^1H\}$ NMR (100 MHz, $CDCl_3$, RT)

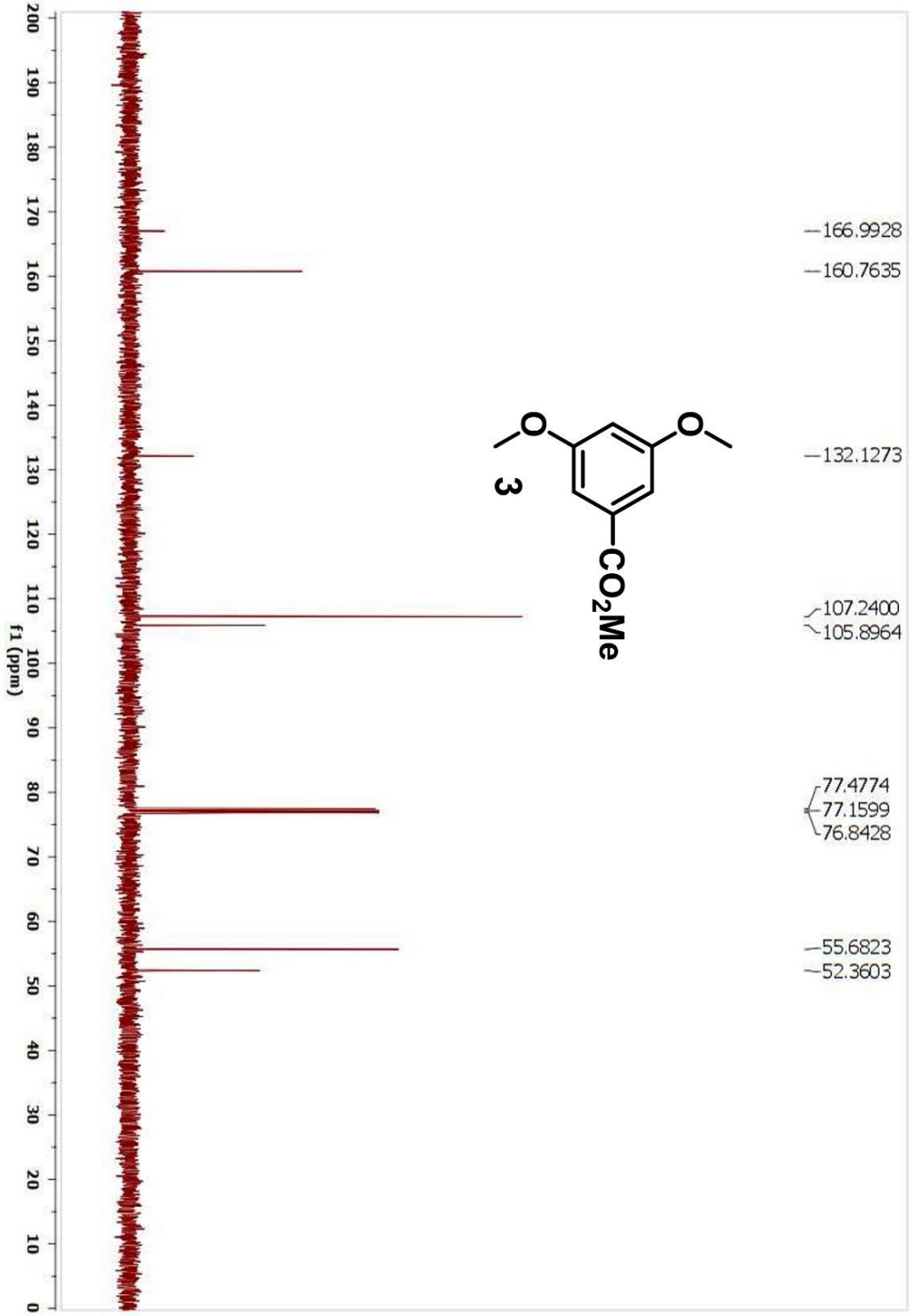

^{1}H NMR (500 MHz, $CDCl_3$, RT)

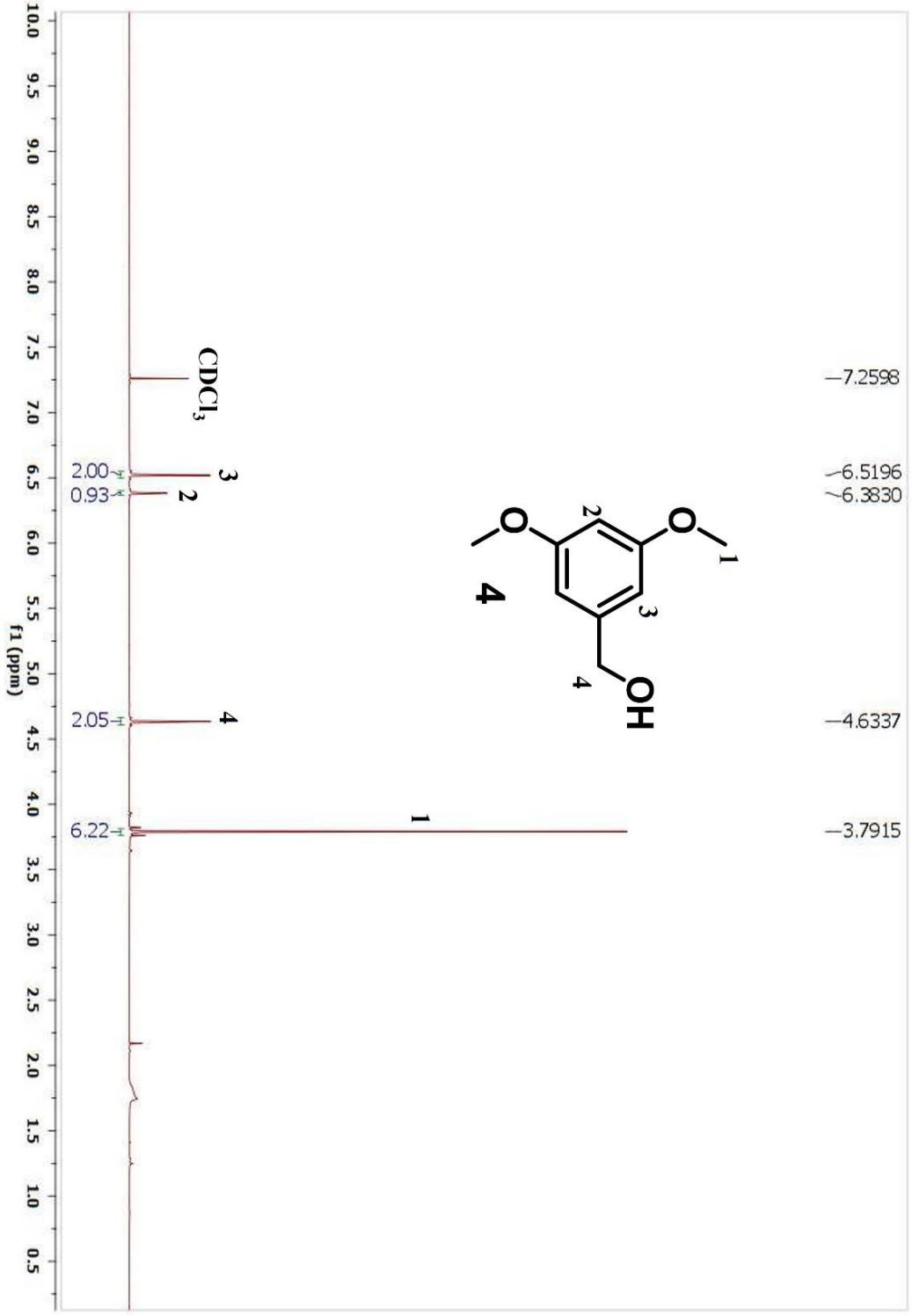

$^{13}C\{^1H\}$ NMR (100 MHz, $CDCl_3$, RT)

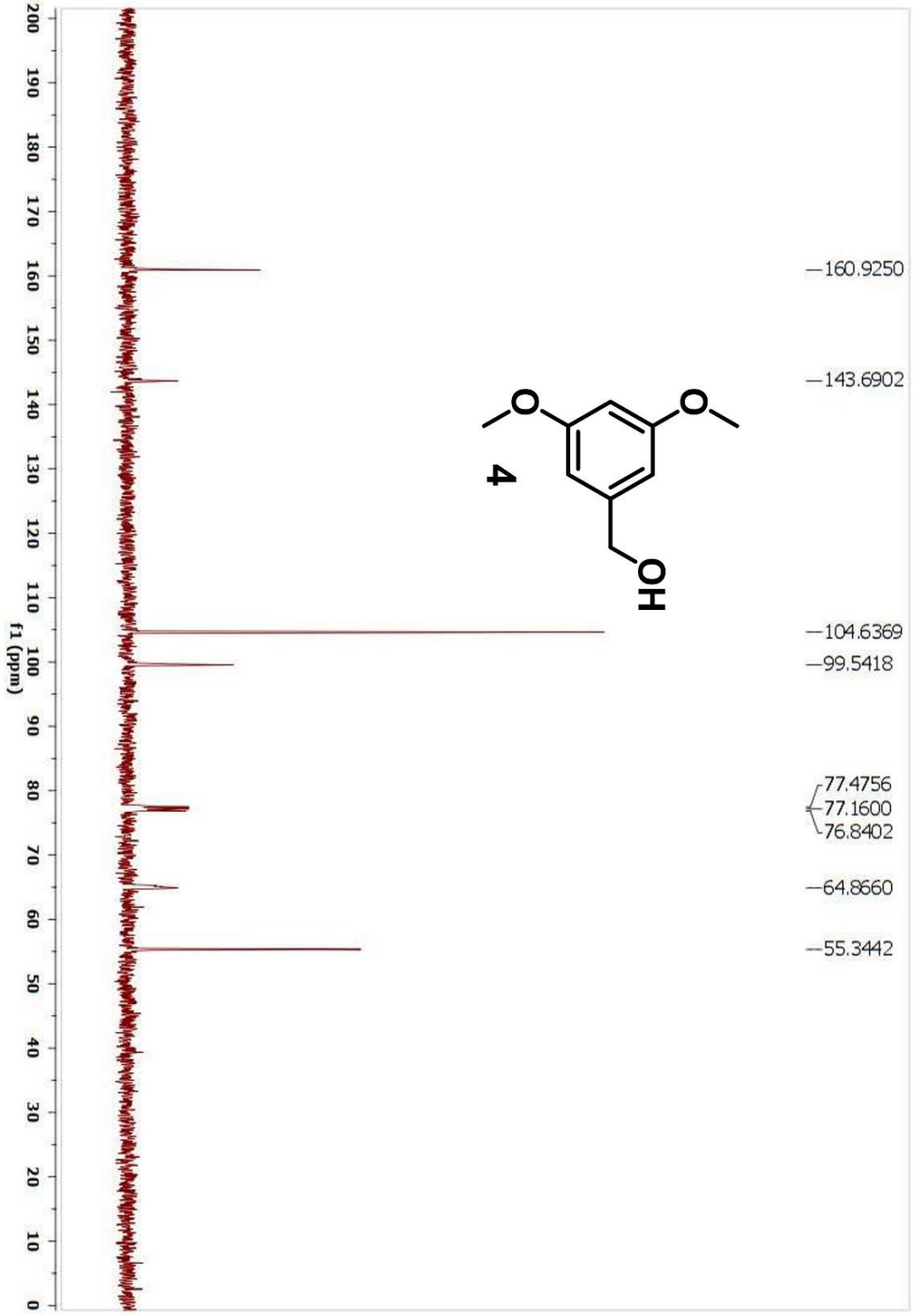

^{1}H NMR (500 MHz, $CDCl_3$, RT)

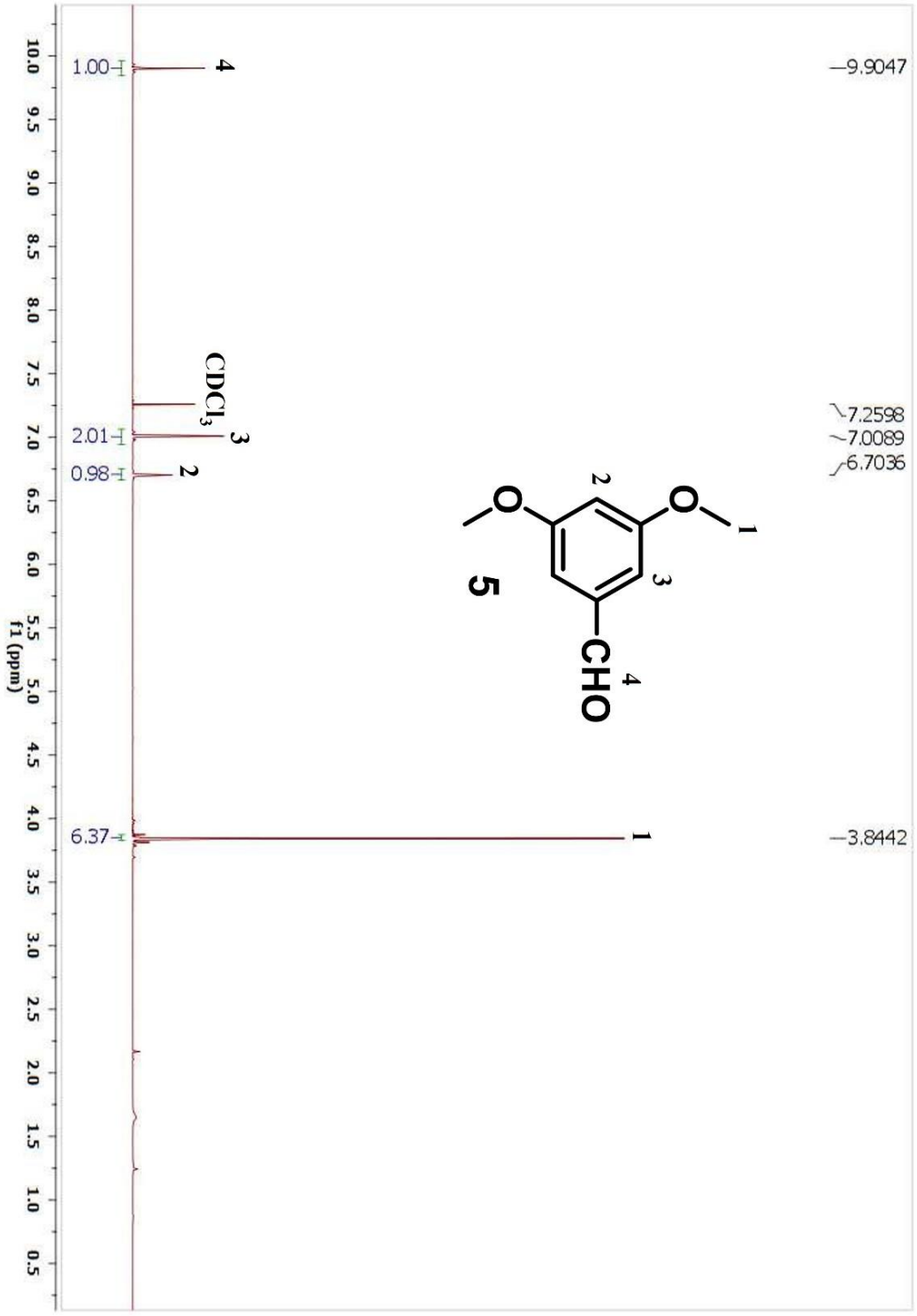

$^{13}C\{^1H\}$ NMR (100 MHz, $CDCl_3$, RT)

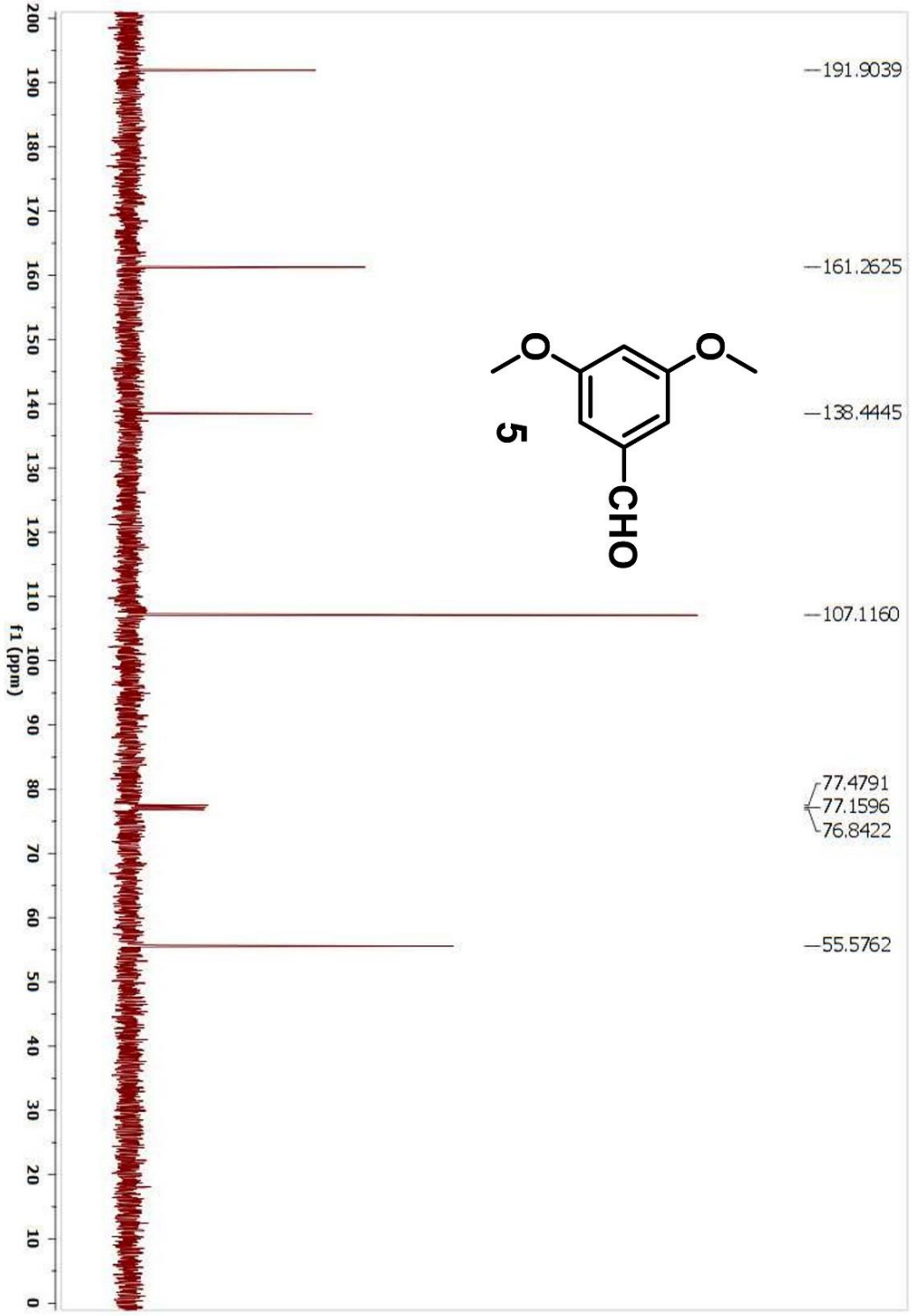

^{1}H NMR (500 MHz, $CDCl_3$, RT)

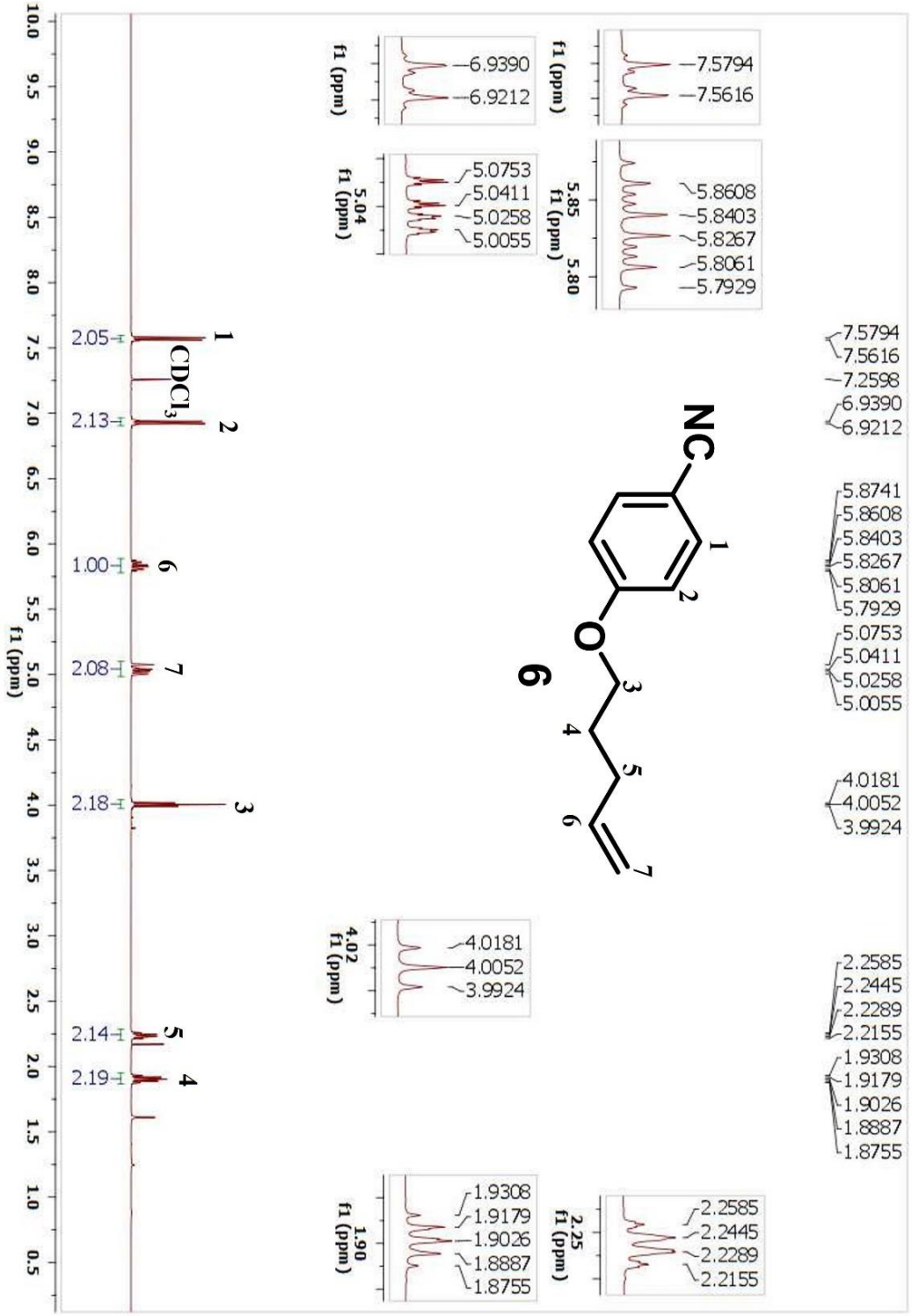

$^{13}C\{^1H\}$ NMR (100 MHz, $CDCl_3$, RT)

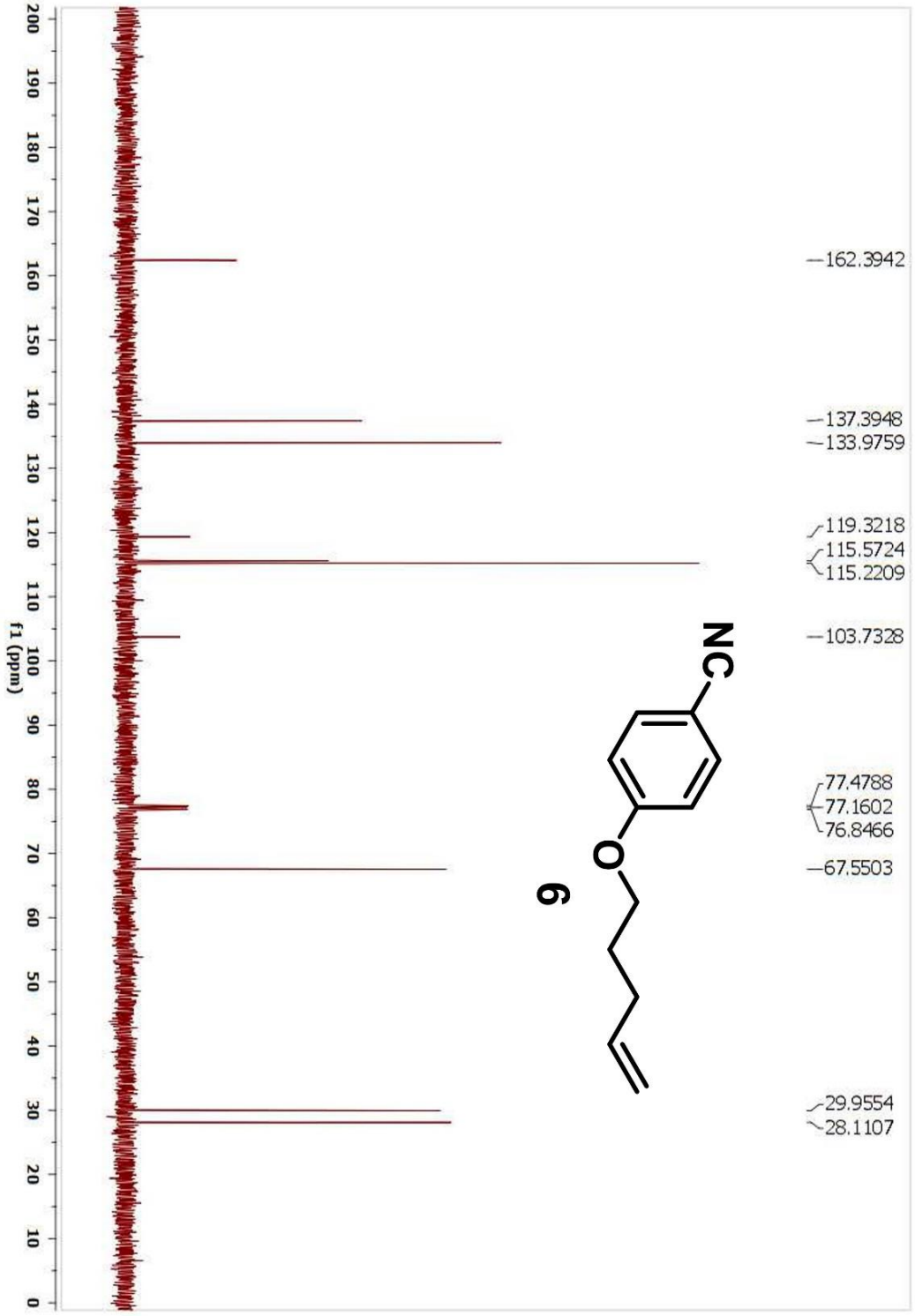

^{1}H NMR (400 MHz, $CDCl_3$, RT)

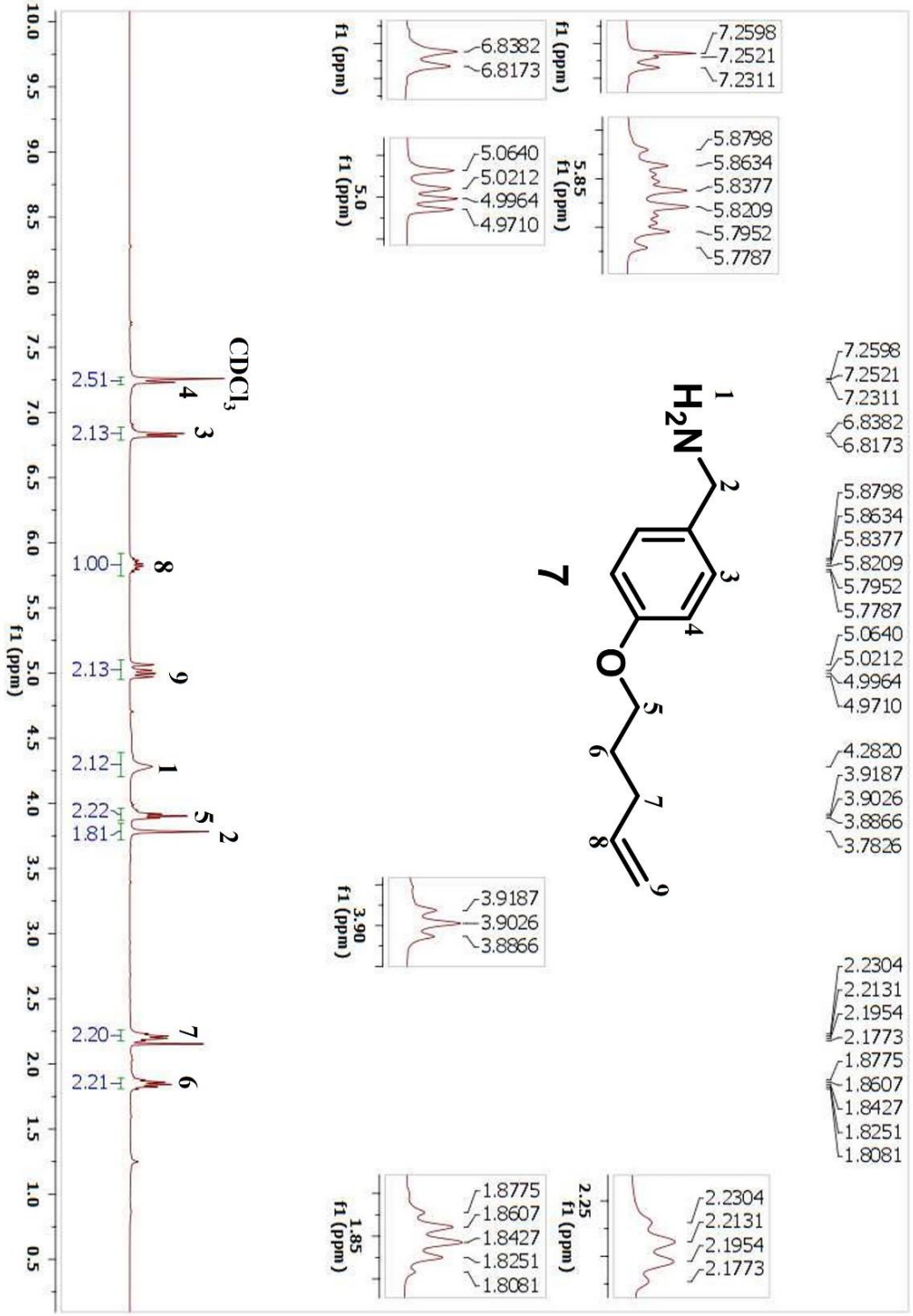

$^{13}C\{^1H\}$ NMR (100 MHz, $CDCl_3$, RT)

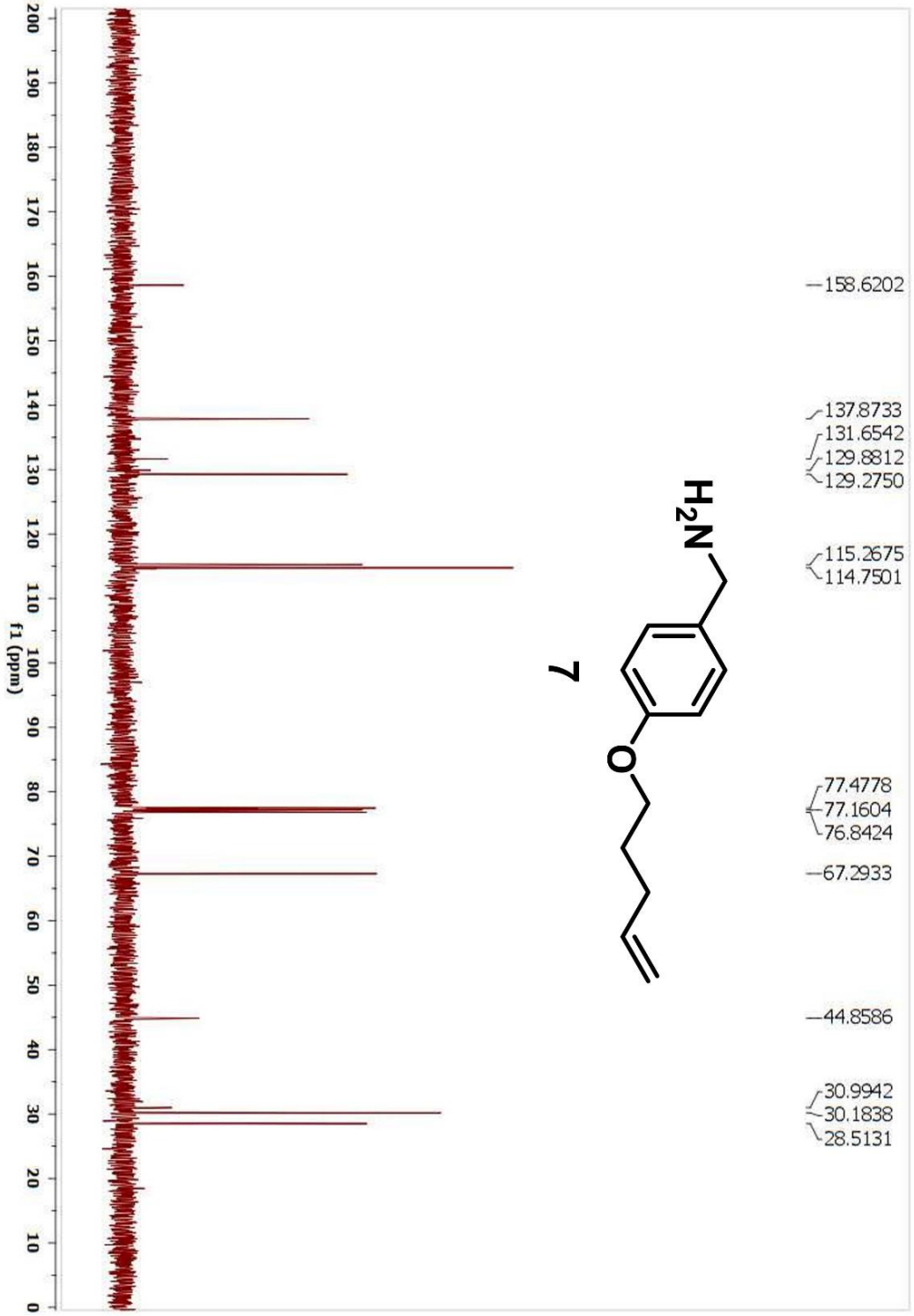

^{1}H NMR (400 MHz, $CDCl_3$, RT)

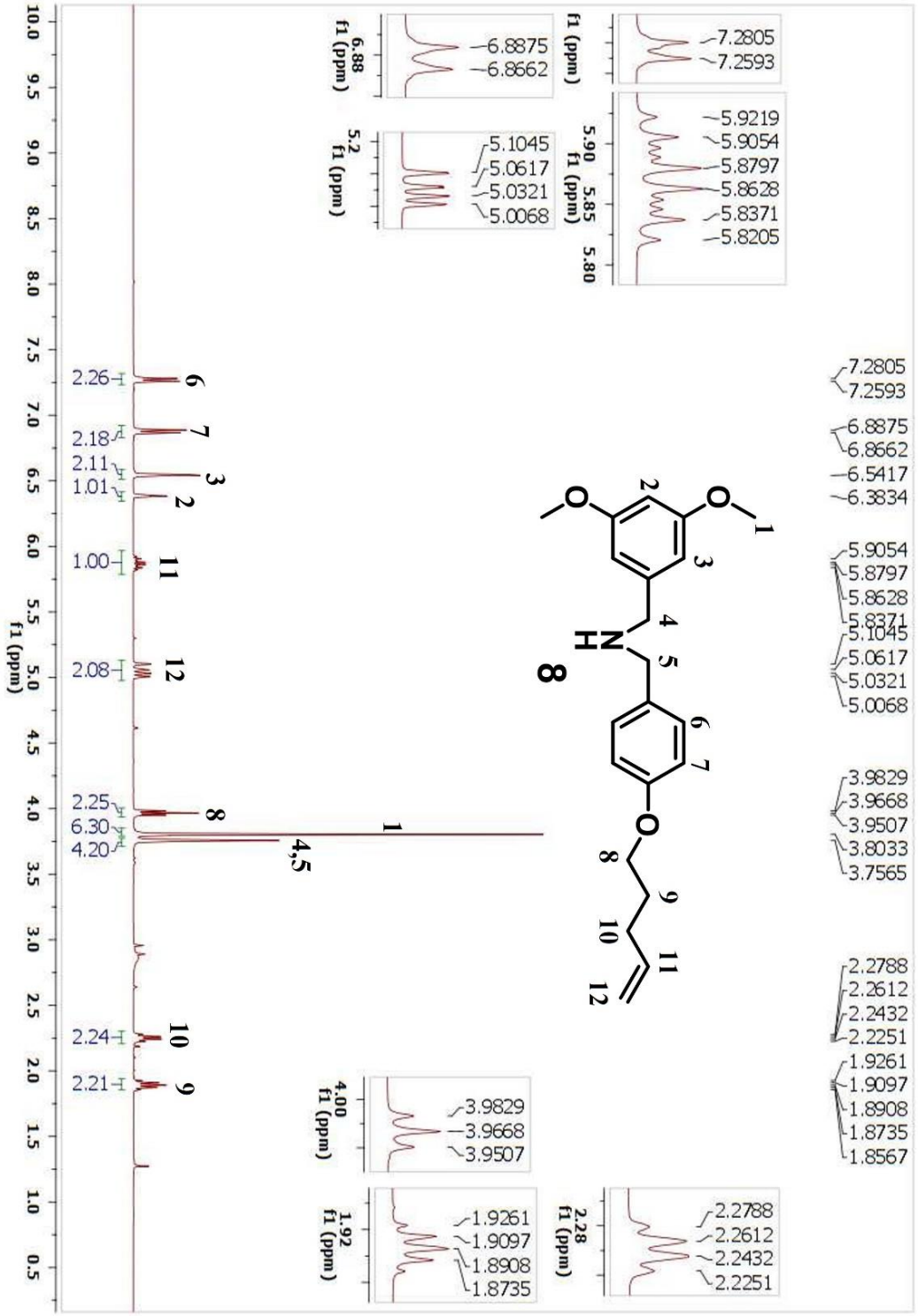

$^{13}C\{^{1}H\}$ NMR (100 MHz, $CDCl_3$, RT)

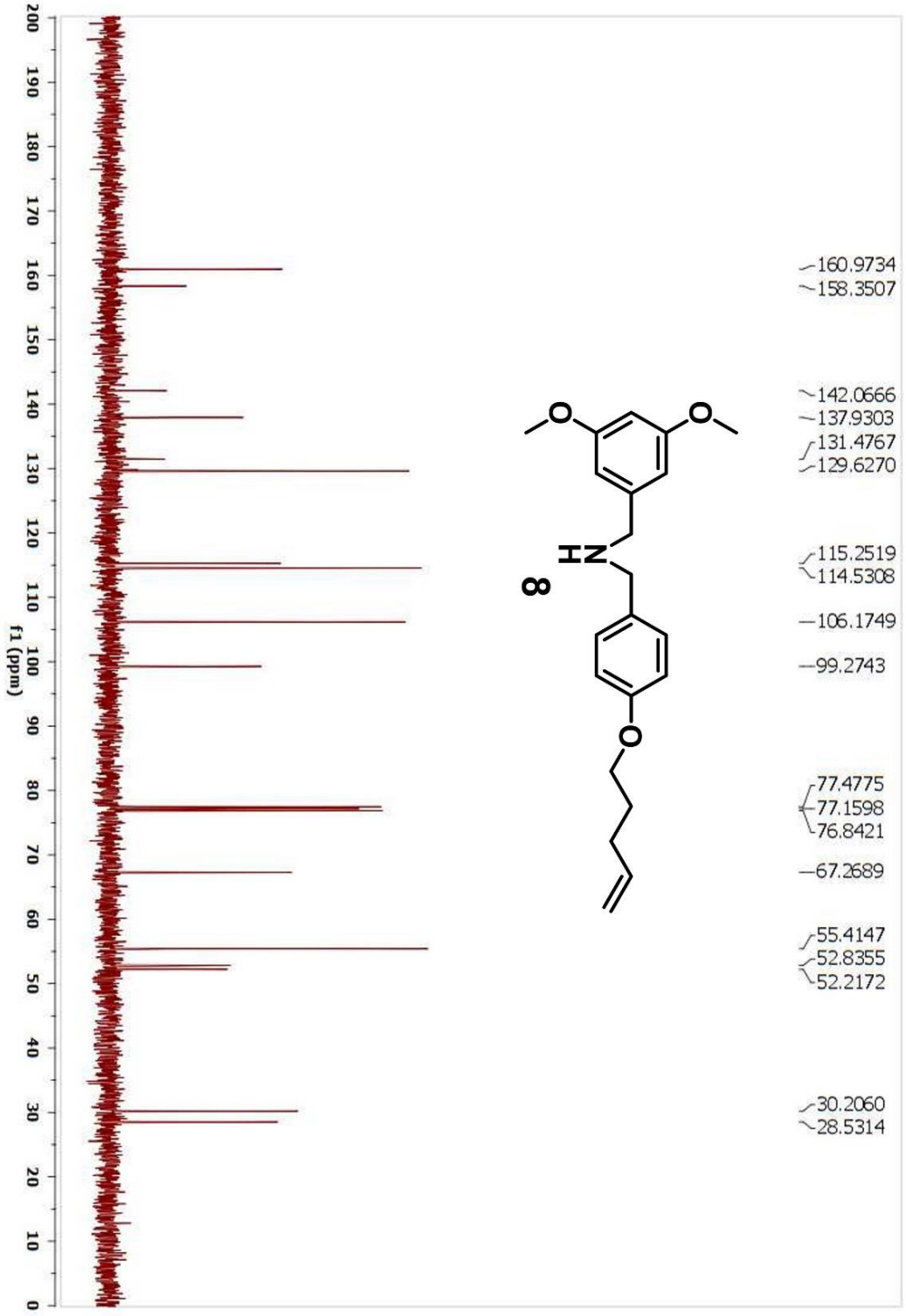

^{1}H NMR (400 MHz, $CDCl_3$, RT)

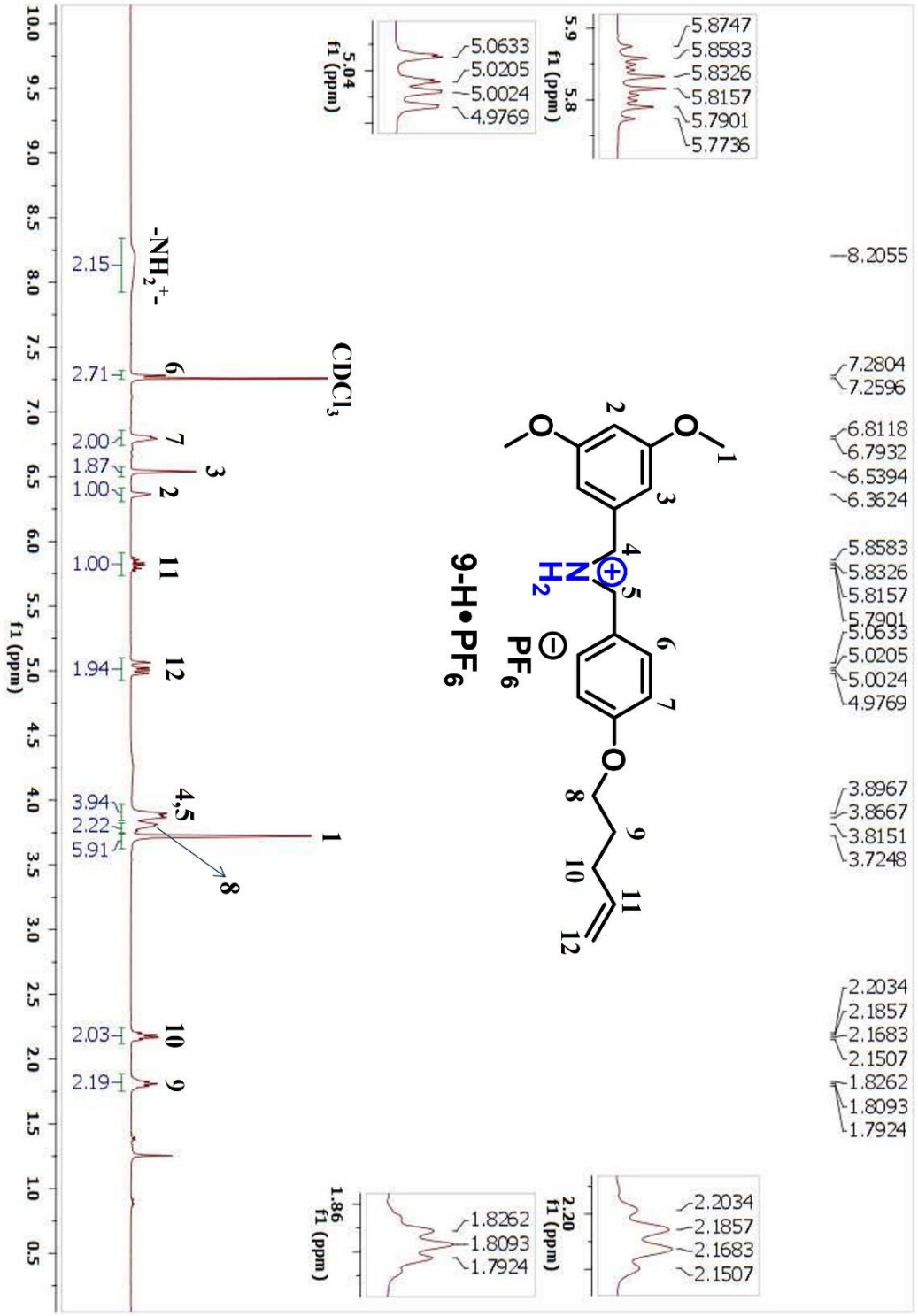

$^{13}C\{^1H\}$ NMR (100 MHz, DMSO-d_6, RT)

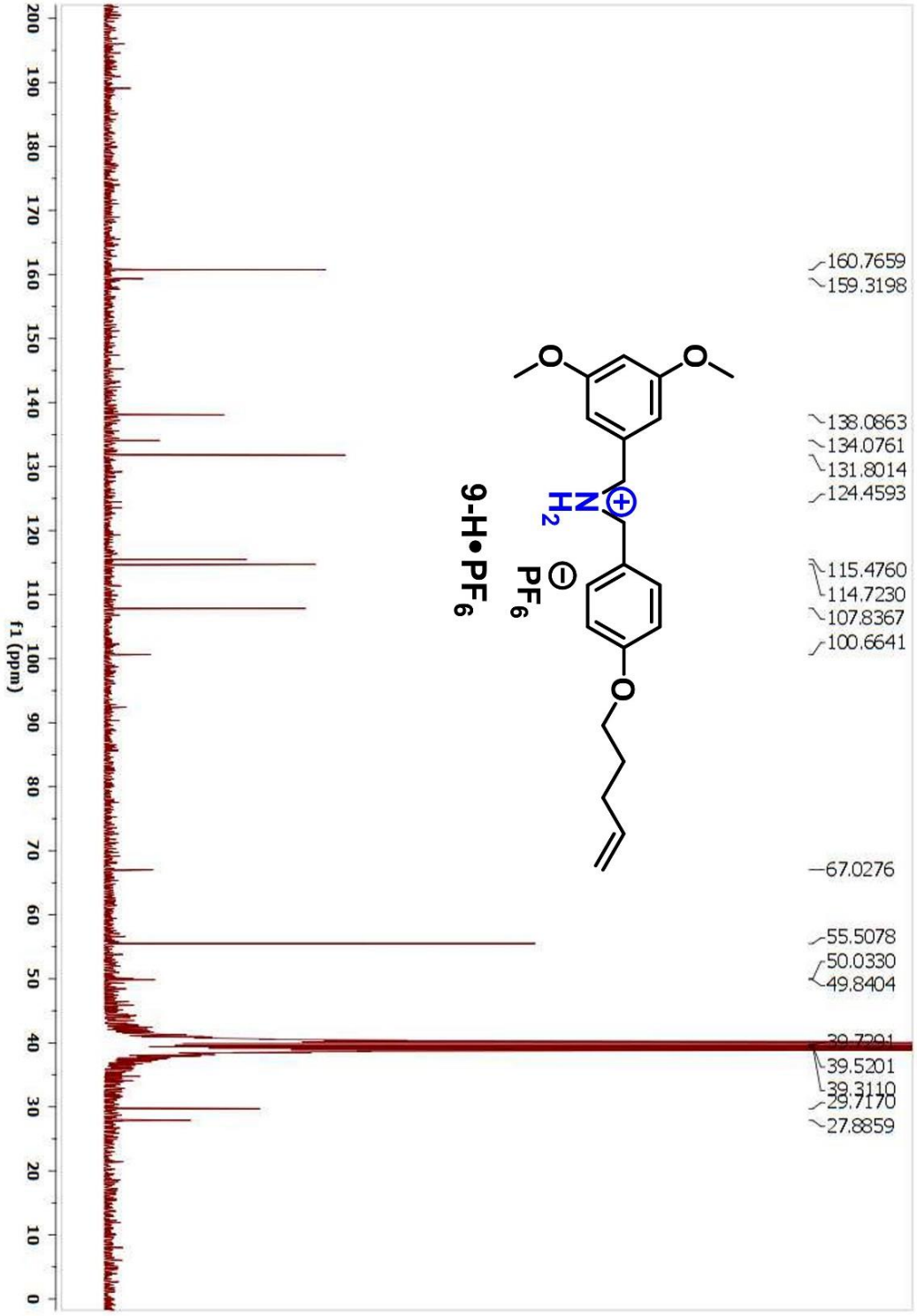

^{1}H NMR (400 MHz, $CDCl_3$, RT)

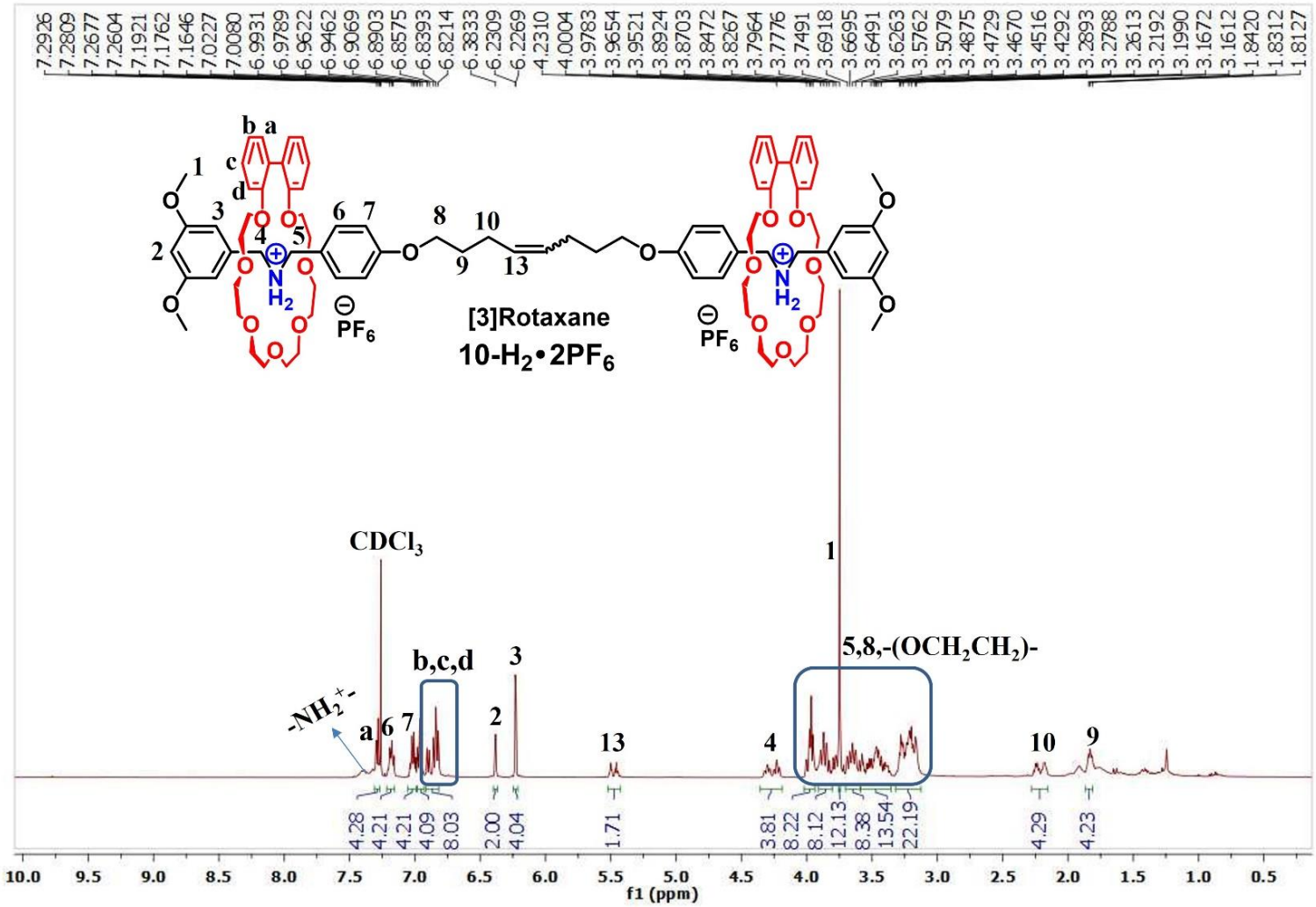

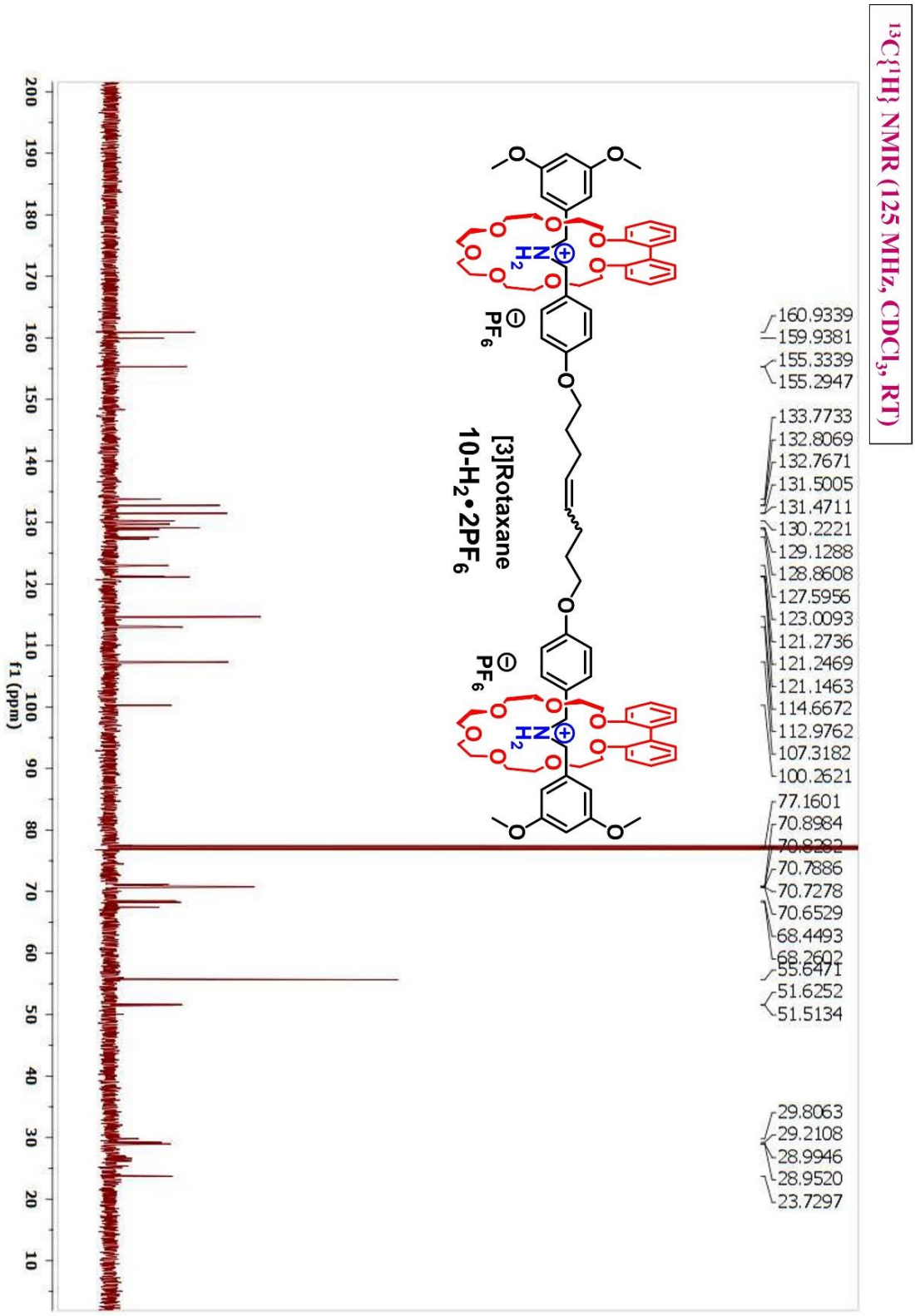
$^{13}C\{^1H\}$ NMR (125 MHz, $CDCl_3$, RT)
[3]Rotaxane
10-H_2•2PF_6
160.9339
159.9381
155.3339
155.2947
133.7733
132.8069
132.7671
131.5005
131.4711
130.2221
129.1288
128.8608
127.5956
123.0093
121.2736
121.2469
121.1463
114.6672
112.9762
107.3182
100.2621
77.1601
70.8984
70.8282
70.7886
70.7278
70.6529
68.4493
68.2602
55.6471
51.6252
51.5134
29.8063
29.2108
28.9946
28.9520
23.7297
f1 (ppm)

^{1}H NMR (400 MHz, $CDCl_3$, RT)

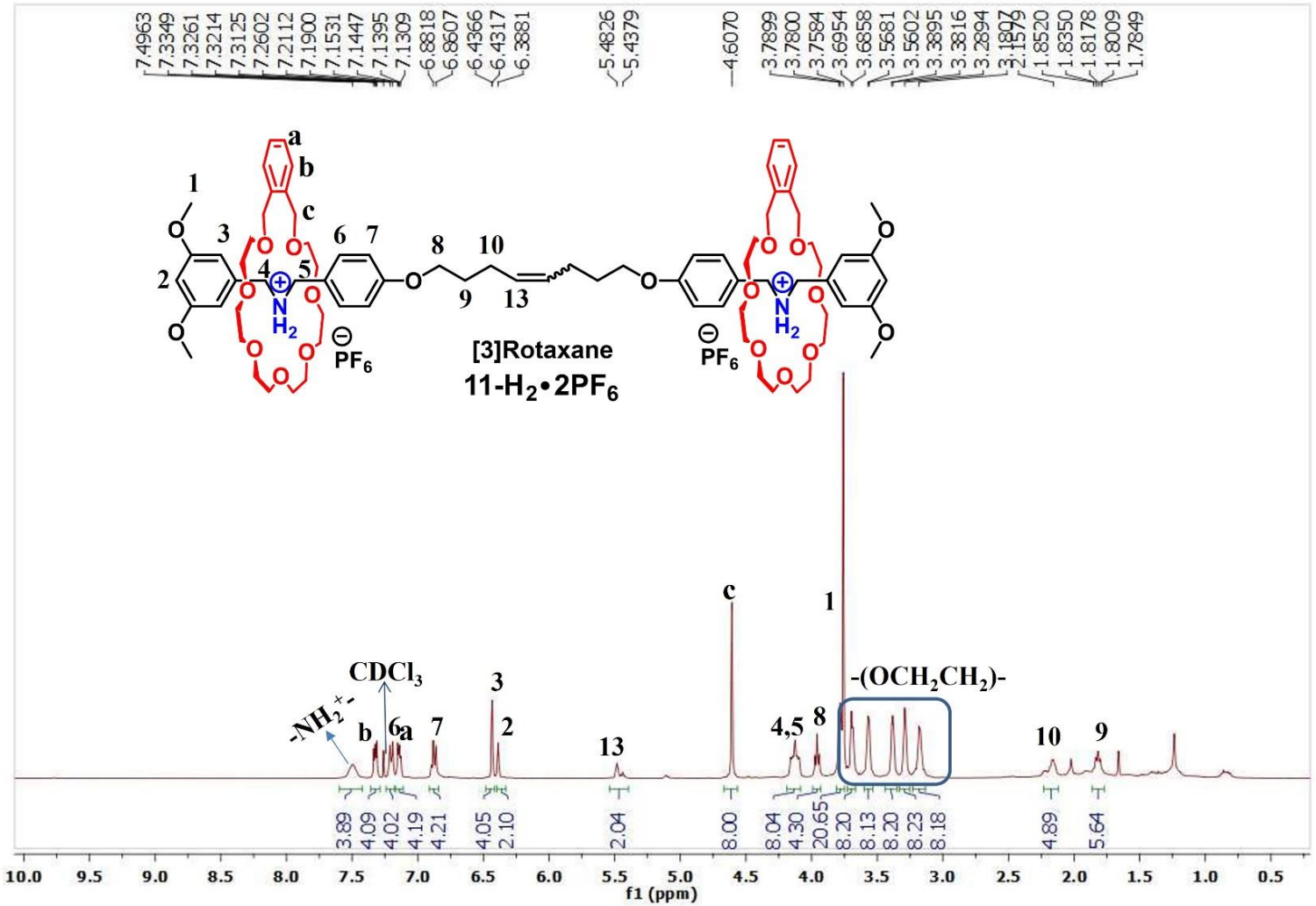

$^{13}C\{^1H\}$ NMR (125 MHz, $CDCl_3$, RT)